Master's Thesis

The Hagedorn temperature at any coupling

Written by *Katharina Hauer*

May 20, 2021

Supervised by
Troels Harmark & Matthias Wilhelm

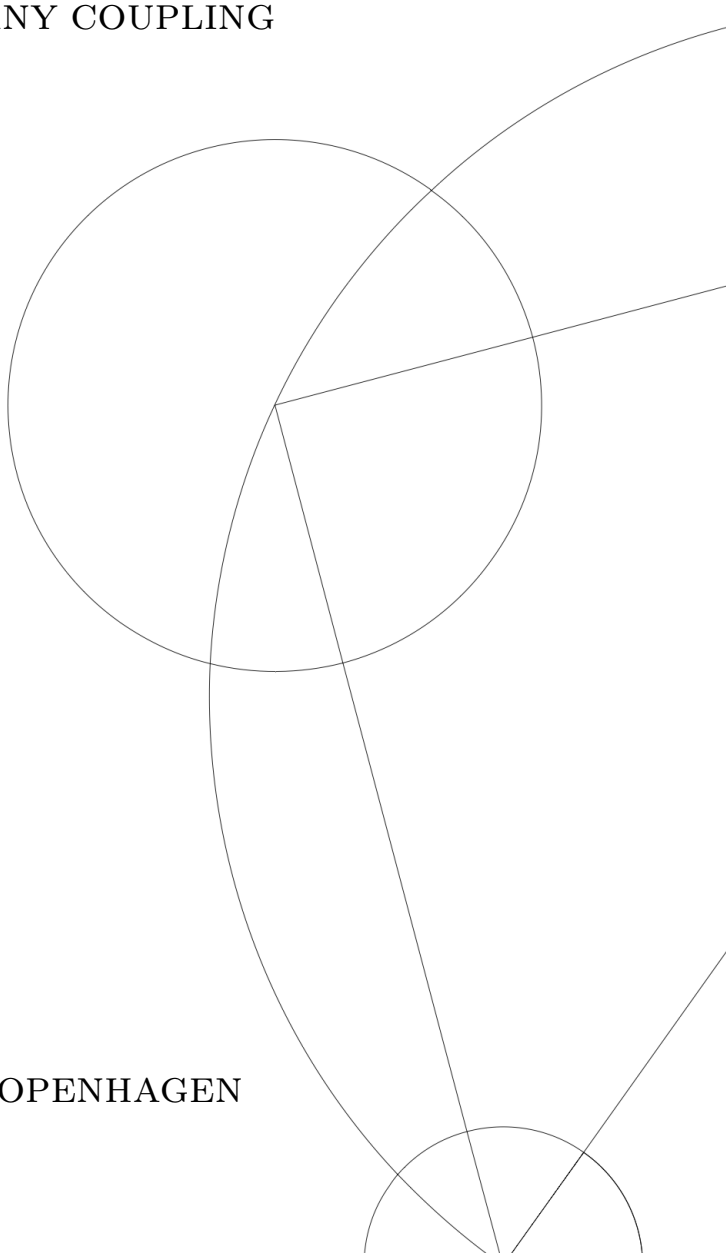

University of Copenhagen

UNIVERSITY OF COPENHAGEN

Faculty:	
Institute:	Niels Bohr Institute
Author(s):	Katharina Hauer
Email:	kathi.hauer@hotmail.com
Title:	The Hagedorn temperature at any coupling
Supervisor(s):	Troels Harmark & Matthias Wilhelm
Handed in:	20.05.2021
Defended:	09.06.2021

Name _____

Signature _____

Date _____

Abstract

The AdS_5/CFT_4 correspondence has the property of integrability, which leads to the formalism of Quantum Spectral Curves (QSC). It is a system of finite-difference equations and can be used to determine the Hagedorn temperature for weak and strong coupling. Based on the method introduced in [1], we solve the QSC numerically in the strong coupling limit at the Hagedorn temperature. We then attempt to find an analytic description of the constituent functions **P** and **Q** of the QSC formalism in the strong coupling limit. The focus of the study lies on the analysis of those functions concerning their dependence of the spectral parameter and the coupling. In order to find an analytic expression we fit the numeric solutions. We apply different ansätze for those functions and compare them regarding numeric stability and their behaviour in the limit $g \to \infty$.

Contents

1 Introduction

In 1975, Hawking found that black holes are radiating energy due to quantum entanglement effects near the event horizon [2]. Quantum states falling into the black hole must collapse and new states are formed which build the Hawking radiation. Thus, the radiated states are independent of the states that were entering the black hole. This is however a contradiction to the principle of information perseverance and is known as the black hole information paradox. It was resolved in 1993, when 't Hooft proposed the idea that incoming states are not destroyed but the information is stored at the horizon of the black hole [3]. Susskind formulated the idea in terms of string theory which is now known as the holographic principle [4]. The first concrete example of the holographic principle was proposed by Maldacena in [5]. He showed that conformal field theories can be described as string theories. Witten's papers [6, 7] generalize Maldacenas paper and state that in fact conformal field theory (CFT) comes naturally at the boundary of Anti-de Sitter (AdS) manifolds. This duality between a gauge theory and a gravity theory is called AdS/CFT correspondence. And since then several such gauge-gravity dualities have been found (see for example [5, 8, 9]). Since its discovery the duality has been the subject of tremendous research in many fields such as nuclear (see e.g. [10, 11, 12]) or condensed matter physics (see e.g. [13, 14]).

The most prominent and most studied realization of the AdS/CFT correspondence is the original proposal by Maldacena [5]. It states that superstring theory of type IIB defined on $AdS_5 \times S^5$ spacetime is dual to $\mathcal{N} = 4$ Super Yang-Mills theory (SYM) in $d = 3 + 1$ dimensions. AdS_5 is referring to a five-dimensional Anti-de Sitter spacetime which has a negative cosmological constant and is a maximally symmetric solution of Einstein's equation. The symmetry is equal to the one of $\mathcal{N} = 4$ SYM with gauge group $SU(N)$. This large number of symmetries makes the gauge theory physically unrealistic, especially the large amount of supersymmetry which has not yet been found confirmed with any observations. However, it shares some qualities with quantum chromodynamics (QCD) which makes it a good model to gain a better understanding of QCD.
A very useful property of the duality is that strongly coupled theories, such as QCD, are corresponding to gravitational theories on weakly curved background metrics. Nonetheless, that also implies that there is a strong string coupling. Non-perturbative methods in type IIB string theory are not well established. Therefore, it is really difficult task to directly prove the equivalence of those theories.

Although the AdS/CFT correspondence is difficult to prove, it still provides new

tools to study strong coupling phenomena. One that has drawn considerable attention is the quark-gluon plasma and its associated phase transition. At low energies quarks and gluons can only occur in certain combinations that form hadrons. However, when they reach a critical temperature they can break free and start behaving like a free gas of quarks and gluons. This "evaporation" is called deconfinement and it is accompanied by a phase transition. It is rather difficult to study the thermodynamic behaviour of QCD (and $SU(N)$ gauge theories) since it is strongly coupled (except at very high energies) and can only be solved using lattice or numeric techniques [1, 15, 16, 17]. However, in the large N limit $SU(N)$ or $U(N)$ gauge theories placed on a compact manifold (such as $\mathcal{N} = 4$ SYM on $\mathbb{R} \times S^3$) have a similar phase transition and are weakly coupled. Therefore, they make good toy models for QCD.

At low temperatures $\mathcal{N} = 4$ SYM on $\mathbb{R} \times S^3$ shows Hagedorn behaviour, which means that the density of states grows exponentially with the energy [15, 18]. However, there is a limiting temperature known as Hagedorn temperature at which the partition function diverges. In case of zero coupling this temperature is equal to the deconfinement temperature, whereas by turning on coupling the deconfinement phase transition occurs even below the temperature for $N \to \infty$ [15]. On the string theory side, at tree level the state density also grows exponentially until it reaches the Hagedorn temperature. And as far as string interactions are concerned, the gas of strings collapses to a black hole. This transition is known as Hawking-Page transition and is connected to the deconfinement phase transition in the gauge theory [6].

Thermodynamics has not really been investigated in the strong coupling limit due to the lack of efficient methods. The solution provides integrability a property that enters the AdS/CFT correspondence naturally. Planar $\mathcal{N} = 4$ SYM has an underlying two-dimensional Heisenberg spin chain at weak coupling which can be solved exactly using the Bethe ansatz (BA) [19]. In the planar limit of the gauge theory string interactions can be neglected and the theory is thus described as a sigma model which is integrable [20]. This makes it possible to study the spectrum and thermodynamic quantities for any values of the coupling. The non-perturbative approach to the spectral problem can be solved with a thermodynamic Bethe ansatz (TBA) and reduced to a finite difference equation system called quantum spectral curves (QSC) [21].

With the QSC formalism it is possible to determine the Hagedorn temperature for any finite coupling by interpolating between the weak and strong coupling limit. This

has been performed numerically by Harmark and Wilhelm in [1]. Continuing their work, it would be of considerable interest to find an analytic formulation of the QSC in the strong coupling limit. Hence, the objective of this thesis is to gain a better understanding of the strong coupling limit. As a foundation, we will use the method and numeric solutions of [1]. We will analyse these solutions that were obtained in the algorithm for strong coupling and further attempt to find an analytic expression by fitting those solutions.

The thesis is divided into five sections, including this introduction. Section 2 will provide the necessary theoretical background and consists of three parts: $\mathcal{N} = 4$ SYM, AdS/CFT and thermodynamics on both theories and finally integrability. The third section presents the results of the research, which are then discussed in the last section.

2 Theory

2.1 $\mathcal{N} = 4$ Super Yang-Mills theory

$\mathcal{N} = 4$ Super Yang-Mills (SYM) theory has been subject of profuse research (see for example [22, 23, 24] and reference herein, which we will follow in this section). The primary reason is that it is dual to type IIB superstring theory according to the AdS/CFT correspondence [5]. But besides that it has many features that are of interest. $\mathcal{N} = 4$ SYM theory is a maximally symmetrical theory which makes it very convenient to work with. It is, among other things, invariant under conformal transformations [25]. Although this is not the case for QCD in general, at high energies the theory becomes asymptotically free which means that it is also conformally invariant in this limit. Hence, $\mathcal{N} = 4$ SYM can be used to examine properties of QCD for high energies.
Conformal invariance, however, implies that there is no running coupling. Thus, there is no mass scale which would allow confinement and further no physical particles like hadrons in QCD. Nevertheless, it is possible to make $\mathcal{N} = 4$ SYM a confining theory by placing it on a compact space, for example on a sphere. In this case, it is possible to use SYM to increase our understanding of QCD and its confinement and the transition to the deconfining phase.

2.1.1 Action and symmetry algebra

The field components of $\mathcal{N} = 4$ SYM are one gauge boson A_μ where $\mu = 1, \dots 4$ are spacetime vector indices, scalar fields ϕ^i where $i = 1 \dots 6$ and Weyl fermions λ^a_α where the indices are $a = 1, \dots 4$, $\alpha = 1, 2$ and $\dot{\alpha} = 1, 2$ representing the left and right chirality $SU(2)_{\mathrm{R}}$ and $SU(2)_{\mathrm{L}}$ respectively. The Lagrangian for $\mathcal{N} = 4$ SYM was first formulated by Brink, Schwarz and Scherk in [26]

$$\begin{aligned}\mathcal{L} = \mathrm{Tr}\Bigg(&\frac{1}{4}F_{\mu\nu}F^{\mu\nu} + \frac{1}{2}D_\mu\phi_i D^\mu\phi^i + \bar{\lambda}^a_{\dot{\alpha}}\sigma_\mu^{\dot{\alpha}\beta}D^\mu\lambda_{\beta a} - i\frac{g_{\mathrm{YM}}}{2}\lambda_{\alpha a}\sigma_i^{ab}\epsilon^{\alpha\beta}[\phi^i, \lambda_{\beta b}] \\ &-i\frac{g_{\mathrm{YM}}}{2}\bar{\lambda}^a_{\dot{\alpha}}\sigma^i_{ab}\epsilon^{\dot{\alpha}\dot{\beta}}[\phi_i, \bar{\lambda}^b_{\dot{\beta}}] - \frac{g^2_{\mathrm{YM}}}{4}[\phi^i, \phi^j][\phi_i, \phi_j]\Bigg).\end{aligned} \tag{1}$$

where $F_{\mu\nu} = \partial_\mu A_\nu - \partial_\nu A_\mu + ig_{YM}[A_\mu, A_\nu]$ is the field strength tensor and $D_\mu \cdot = \partial_\mu \cdot -ig[A_\mu, \cdot]$ the covariant derivative. The matrices σ^μ and σ^m are the chiral projections of the γ-matrices in four or six dimensions, respectively. Furthermore, the theory is gauge invariant and one can choose the gauge group, which is in our case $SU(N)$ or $U(N)$. The Yang-Mills coupling constant is denoted as g_{YM}. Its β-function vanishes for all couplings. This was first shown for up to three-loop order by [27, 28, 29, 30] and then

generalized by [26, 31, 32] to all loop orders using light cone superspace. This suggests that the theory is UV finite for all loop orders.

The underlying algebra of $\mathcal{N} = 4$ SYM is the superconformal algebra $PSU(2,2|4)$. It is maximally symmetric which implies $\mathcal{N} = 4$ supersymmetry, conformal symmetry and R-symmetry [33].
The conformal algebra $SU(2,2) \simeq SO(2,4)$ is invariant under Poincaré transformations, which includes translations and Lorentz transformations. Furthermore, It is invariant under dilatations and special conformal transformations which can be thought as a composition of transformation that has first an inversion, then a translation, then another inversion. The dilatation operator will be of special interest in this work since it gives the scaling dimensions of operators, as will be discussed below.
Supersymmetry allows us to transform between bosons and fermions. It is the natural extension of Poincaré symmetry as stated by Haag, Sohnius and Lopuszanski [34]. Its generators are supercharges $Q_{a\alpha}$ and $\tilde{Q}^a_{\dot{\alpha}}$ as well as superconformal charges S^a_α, $\tilde{S}_{\dot{\alpha}a}$, where $\alpha, \dot{\alpha} = 1, 2$ and $a = 1, \dots 4$. They all behave in a fermionic way.
R-symmetry, which is $SU(4) \simeq SO(6)$, is the manifestation of a global rotational invariance of the supercharges and follows

$$Q^a_\alpha \mapsto Q^{a'}_\alpha = R^a_b Q^b_a, \qquad \bar{Q}_{a\dot{\alpha}} \mapsto \bar{Q}'_{a\dot{\alpha}} = \bar{Q}_{b\dot{\alpha}} (R^\dagger)^b_a. \tag{2}$$

$R \in SU(4)$ are the generators of this symmetry in case of $\mathcal{N} = 4$ SYM. It is non-Abelian and it does not commute with supersymmetry.

The superconformal algebra $PSU(2,2|4)$ has a bosonic subalgebra $SU(2,2) \times SU(4)$. It is of rank six and can thus be represented as a sextuplet $(\Delta, S_1, S_2; J_1, J_2, J_3)$. It includes the dimension of the operator Δ, the charges of the Lorentz group S_1 and S_2 and the charges of R-symmetry J_1, J_2 and J_3.

2.1.2 Local operators

Local operators are constructed out of products and linear combinations of fundamental fields and their derivatives. One can distinguish two types of operators: primary and descendant. Descendant operators are constructed from derivatives of primary operators and together they build a set of irreducible representations for $PSU(2,2|4)$ [33]. Local operators can be regarded as states of the theory which can be made clear as in the following. Consider spherical coordinates on $\mathbb{R}^d$

$$ds^2 = dr^2 + r^2 d\Omega^2_{d-1}, \tag{3}$$

By identifying $r = e^\tau$ we obtain a cylinder $\mathbb{R} \times S^{d-1}$ instead of $\mathbb{R}^d$. With that the metric reduces to

$$ds^2 = e^{2\tau} \left(d\tau^2 + d\Omega_{d-1}^2 \right) \tag{4}$$

which is just a Weyl transformation of eq. (3). Putting a local operator at the centre of the sphere in $\mathbb{R}^d$ can then be viewed as preparing a state at $\tau = -\infty$. Time translations for the operators are described by the dilatation operator on $\mathbb{R}$ whereas time translations of the states on $\mathbb{R} \times S^{d-1}$ are described by the Hamiltonian. This translation between states and operators is known as the state-operator map.

Each of the local operators $\mathcal{O}(x)$ has a dimension Δ. This dimension appears in scalings such as $x \to \lambda x$ where $\mathcal{O}(x)$ transforms as

$$\mathcal{O}(x) \to \lambda^{-\Delta} \mathcal{O}(\lambda x). \tag{5}$$

The generator of rescalings is the dilatation operator D for which then holds

$$\mathcal{O}(x) \to \lambda^{-iD} \mathcal{O}(x) \lambda^{iD}. \tag{6}$$

By considering the infinitesimal transformation, one can find the action of D on $\mathcal{O}(x)$

$$[D, \mathcal{O}(x)] = i \left(-\Delta + x \frac{\partial}{\partial x} \right) \mathcal{O}(x). \tag{7}$$

For operators at $x = 0$ this implies

$$[D, \mathcal{O}(0)] = -i\Delta \mathcal{O}(0). \tag{8}$$

The dimension of the operator Δ can be shifted up and down by acting on $\mathcal{O}(0)$ with other generators. One of those is the generator of translations P_μ. Using the commutation relation $[D, P_\mu] = -iP_\mu$ one can calculate

$$\begin{aligned} [D, [P_\mu, \mathcal{O}(0)]] =& [[D, P_\mu], \mathcal{O}(0)] + [P_\mu, [D, \mathcal{O}(0)]] = -i[P_\mu, \mathcal{O}(0)] - i\Delta[P_\mu, \mathcal{O}(0)] \\ =& -i(\Delta + 1)[P_\mu, \mathcal{O}(0)]. \end{aligned} \tag{9}$$

This calculation shows that the dimension of the operator $\mathcal{O}$ is raised by 1. The other operator is the generator of special conformal transformations K_μ which is connected to the dilation operator as $[D, K_\mu] = iK_\mu$. Doing a similar calculation to eq. (9) one finds

$$[D, [K_\mu, \mathcal{O}(0)]] = -i(\Delta - 1)[K_\mu, \mathcal{O}(0)] \tag{10}$$

that the dimension of the operator $\mathcal{O}$ is lowered by 1. Hence, it is possible to find a lower limit for the dimension in each representation which is reached if

$$[K_\mu, \tilde{\mathcal{O}}(0)] = 0. \tag{11}$$

Local operators satisfying eq. (11) are called primary operators. They have the lowest possible dimension and are thus eigenstates of special conformal transformations [33].

Introducing supersymmetry, there exists a similar picture. By commuting a local operator $\mathcal{O}(0)$ with the superconformal charges S^a_α, $\tilde{S}_{\dot{\alpha}a}$ lowers the dimension by $\frac{1}{2}$. In contrast acting with the supercharges $Q_{a\alpha}$ and $\tilde{Q}^a_{\dot{\alpha}}$ the dimension is increased by $\frac{1}{2}$. Furthermore, primary operators have to satisfy

$$[S^a_\alpha, \mathcal{O}(0)] = [\tilde{S}_{\dot{\alpha}a}, \mathcal{O}(0)] = 0. \tag{12}$$

It is a more general lower boundary condition for the scaling dimension and it implies eq. (11) due to the anti-commutation relations

$$[S^a_\alpha, K_\mu] = [\tilde{S}_{\dot{\alpha}a}, K_\mu] = 0. \tag{13}$$

Fields of $\mathcal{N} = 4$ SYM are defined in the adjoint representation. Therefore, they transform in a covariant way

$$\chi(x) \to \chi(x) + [\varepsilon(x), \chi(x)], \tag{14}$$

where χ is a local field and ε the local gauge transformation. From those fields one can construct new covariant fields by taking the covariant derivative

$$\mathcal{D}_\mu \chi(x) \equiv \partial_\mu \chi(x) - [A_\mu(x), \chi(x)] \tag{15}$$

where $A_\mu(x) \to A_\mu(x) + \partial_\mu \varepsilon(x) + [\varepsilon(x), A_\mu(x)]$. To obtain a gauge-invariant operator one can take the trace of products of covariant fields (or their covariant derivatives)

$$\mathcal{O}(x) = \mathrm{Tr}[\chi_1(x)\chi_2(x)\dots\chi_L(x)]. \tag{16}$$

Such operators are called single-trace operators and their products are multi-trace operators. An example is the operator

$$\mathcal{O}(x) = \mathrm{Tr}\Big[X^k\Big], \tag{17}$$

where X is a complex scalar field of the form $X = \frac{1}{\sqrt{2}}(\phi^5 + i\phi^6)$ and $k > 2$ since the trace of a scalar field is zero [33]. Equation (17) is of special interest since it is a chiral primary operator and has a scaling dimension of $\Delta = k$. Chiral primaries are a general set of operators with symmetrized indices and are traceless in the sense that the trace of any two indices vanishes. These properties leave their dimension invariant when introducing quantum corrections, which will be explained further below.

2.1.3 Large N factorization

As mention above, all the fields are in the adjoint representation to provide gauge-invariance. Consider for example only the scalar fields in eq. (1). We can build a toy Lagrangian for scalar fields and their coupling g that reads

$$\begin{aligned}\mathcal{L} &= -\frac{1}{2}\operatorname{Tr}(\partial_\mu\phi\partial^\mu\phi) + g\operatorname{Tr}\left(\phi^3\right) + g^2\operatorname{Tr}\left(\phi^4\right) \\ &= \frac{1}{g^2}\left(-\frac{1}{2}\operatorname{Tr}\left(\partial_\mu\tilde{\phi}\partial^\mu\tilde{\phi}\right) + \operatorname{Tr}\left(\tilde{\phi}^3\right) + \operatorname{Tr}\left(\tilde{\phi}^4\right)\right),\end{aligned} \tag{18}$$

where we obtained the last equality by rescaling $\tilde{\phi} = g\phi$. By introducing the 't Hooft coupling $\lambda = g^2N$, we can further go to the limit where $N \to \infty$ and λ is kept fixed. This is called the 't Hooft limit [35]. In this case the propagator of two scalar fields reduces to

$$\langle\tilde{\phi}^i_j\tilde{\phi}^k_l\rangle \propto \frac{\lambda}{N}\delta^i_l\delta^k_j. \tag{19}$$

Feynman diagrams presenting such propagators scale as

$$\left(\frac{N}{\lambda}\right)^V\left(\frac{\lambda}{N}\right)^E N^F = \left(\frac{N}{\lambda}\right)^\chi \lambda^F. \tag{20}$$

Here V is the number of vertices in the diagram, E the number of propagators and F the number of loops. They are the constituents of the minimal Euler character $\chi = V+F-E$ and are connected to the genus of the surface g as $\chi = 2-2g$. With that the correlation function can be expanded in terms of N

$$\langle\mathcal{O}_1\dots\mathcal{O}_n\rangle = \sum_{g=0}^{\infty} N^{2-n-2g} f_g(\lambda), \tag{21}$$

where $\mathcal{O}_i$ represent single trace operators. By sending $N \to \infty$ the contributing diagrams are the ones with $g = 0$ which are the planar diagrams. Equation (21) is known as the large N expansion and can be connected to a similar expansion in string theory which suggests the AdS/CFT correspondence and will be further discussed in section 2.2.1.

2.1.4 Anomalous dimension

In general, the scaling dimension of operators Δ depends on the coupling g_{YM}. When considering the free theory, which means there is no interaction between field components, the scaling dimension is equal to the bare dimension Δ_0. However, in the case of quantum corrections, the dimension Δ obtains an additional term $\Delta = \Delta_0 + \delta\Delta$. The correction to the dimension $\delta\Delta$ is called anomalous dimension.

In the following we are going to consider the 't Hooft limit which ensures that only planar graphs contribute at one-loop level since all others are suppressed by $\frac{1}{N^2}$. Further, if the 't Hooft coupling is small $\lambda \ll 1$ it is ensured that the anomalous dimension is small compared to the bare dimension $\delta\Delta \ll \Delta_0$.

The anomalous dimension can be determined by the two-point correlation function of the operator with itself. As an example consider the bosonic subalgebra again with a simple single trace operator for L scalar fields

$$\mathcal{O}(x) = \frac{(4\pi^2)^{L/2}}{\sqrt{C_{I_1 I_2 \dots I_L}} N^{L/2}} \operatorname{Tr}(\phi_{I_1} \phi_{I_2} \cdots \phi_{I_L}). \tag{22}$$

The factor before the trace is for normalization where $C_{I_1 I_2 \dots I_L}$ is a symmetry factor. The operator has L indices where each has an $SO(6)$ tensor and it is mapped to a space

$$\mathcal{H} = \mathcal{V}_1 \otimes \cdots \otimes \mathcal{V}_L, \qquad \mathcal{V}_l \in \mathbb{R}^6. \tag{23}$$

Therefore, one can conclude that the anomalous dimension should also live on a space as in eq. (23). Consequently, the anomalous dimension $\delta\Delta$ should be the eigenvalue of some $6^L \times 6^L$ matrix Γ.

The matrix Γ can be calculated by considering all the relevant planar Feynman diagrams at one-loop order which has been done several times as in [19, 36, 37, 38]. The quantum correction term then delivers the anomalous dimension matrix which has been found to be [19]

$$\Gamma = \frac{\lambda}{16\pi^2} \sum_{l=1}^{L} \left(K_{l,l+1} + 2 - 2P_{l,l+1} \right). \tag{24}$$

It contains the 't Hooft coupling $\lambda \equiv g_{\mathrm{YM}}^2 N$ and two operators which act on the color indices. $K_{l,l+1}$ is called the trace operator and contracts color indices I, J

$$K_{l,l+1} \delta^{J_1}_{I_1} \cdots \delta^{J_l}_{I_l} \delta^{J_{l+1}}_{I_{l+1}} \cdots \delta^{J_L}_{I_L} = \delta^{J_1}_{I_1} \cdots \delta_{I_l I_{l+1}} \delta^{J_l J_{l+1}} \cdots \delta^{J_L}_{I_L}. \tag{25}$$

$P_{l,l+1}$ exchanges color indices

$$P_{l,l+1} \delta^{J_1}_{I_1} \cdots \delta^{J_l}_{I_l} \delta^{J_{l+1}}_{I_{l+1}} \cdots \delta^{J_L}_{I_L} = \delta^{J_1}_{I_1} \cdots \delta^{J_{l+1}}_{I_l} \delta^{J_l}_{I_{l+1}} \cdots \delta^{J_L}_{I_L}. \tag{26}$$

Therefore, it is called permutation operator. Acting with Γ on an operator gives the anomalous dimension $\delta\Delta$. As an example, let us first consider chiral primaries. The action of the trace operator eq. (25) on chiral primaries as defined in eq. (17) vanishes since they are traceless by definition. Furthermore, they are invariant under color exchanges, since we look at symmetrized indices inside the trace. Thus,

$$\Gamma \mathcal{O}_{\mathrm{Primary}}(x) = 0 \tag{27}$$

which proves that chiral primaries are not affected by quantum corrections and thus have a protected dimension. However, there are also operators, for which this is not the case. Consider for example the Konishi operator

$$\mathcal{O}_{\text{Konishi}}(x) = \sum_{i=1}^{6} \text{Tr}(\phi_i \phi_i). \tag{28}$$

It is invariant under color exchange as well, but acting on it with $K_{l,l+1}$ results in [36]

$$K_{l,l+1}\mathcal{O}_{\text{Konishi}}(x) = 6\mathcal{O}_{\text{Konishi}}(x). \tag{29}$$

The anomalous dimension is then obtained by eq. (24)

$$\delta\Delta_{\text{Konishi}} = \frac{3\lambda}{4\pi^2}. \tag{30}$$

Now let us get back to the Hilbert space for the anomalous dimension eq. (23), which is formed by the $SO(6)$ singlets of scalar fields. This space is in fact the same space as for a spin chain of length L and with $SO(6)$ symmetry at each site [36]. Thus, one can regard the anomalous matrix Γ as the Hamiltonian of this spin chain. Consequently, $\mathcal{N} = 4$ SYM has a spin chain as an underlying model. Spin chains are exactly solvable and therefore also $\mathcal{N} = 4$ SYM. This property is called integrability and will be discussed in more detail in section 2.3.

2.2 Thermodynamic behaviour and Hagedorn temperature

$\mathcal{N} = 4$ SYM theory, as discussed so far, has no temperature dependence. By putting the theory on a compactified spacetime it becomes dependent on the temperature in a non-trivial way [7]. This leads to two different descriptions of the thermodynamic behaviour for high and low temperatures. They are connected by a phase transition which is suspected to be the analogue of the confinement-deconfinement transition observed in QCD [7]. Before discussing the thermodynamic behaviour, we are going to introduce the AdS/CFT correspondence between $\mathcal{N} = 4$ SYM on $\mathbb{R} \times S^3$ and type IIB string theory on $AdS_5 \times S^5$. It allows to combine thermodynamics in the gauge theory with the one of string theory. Thus, we are able to find new insights especially concerning the limit of strong coupling. A significant finding is that the deconfinement phase transition is dual to the Hawking-Page transition [15, 39]. Both phase transitions have a limiting temperature at which the low temperature phase stops existing. This temperature is known as Hagedorn temperature. It is accompanied with an exponential growth of the density of states which is hence referred to as Hagedorn behaviour.

2.2.1 AdS/CFT correspondence

The AdS/CFT correspondence relates a conformal field theory to a quantum gravity. Different types of dualities have been found. However, the one that is relevant here is the one that relates $\mathcal{N} = 4$ SYM in $d = 4$ dimensions and with gauge group $SU(N)$ to type IIB string theory on $AdS_5 \times S^5$. The discovery in [5] was motivated by string theory as the description of D3-branes and gives hints that those theories describe the same physics. This and some of the most important features will be briefly reviewed in this section.

Anti-de Sitter Spacetime

The Lorentzian AdS_{d+1} spacetime is a hyperboloid which is embedded in a space with one additional dimension $\mathbb{R}^{d,2}$

$$-(X^0)^2 + (X^1)^2 + \cdots + (X^d)^2 - (X^{d+1})^2 = -R^2, \tag{31}$$

where $X^0 > 0$ and R is the radius of AdS. It is convenient to introduce the coordinates

$$X^0 = R \cos t \cosh \rho, \tag{32}$$

$$X^\mu = R\Omega^\mu \sinh \rho, \tag{33}$$

$$X^{d+1} = -R \sin t \cosh \rho, \tag{34}$$

with Ω^μ are the coordinates of a unit sphere for $\mu = 1, \ldots, d$. With those coordinates the metric is

$$ds^2 = R^2 \left(-\cosh^2 \rho \, dt^2 + d\rho^2 + \sinh^2 \rho \, d\Omega_{d-1}^2 \right), \tag{35}$$

with the time coordinate $t \in \mathbb{R}$ and the radial coordinate $\rho \in [0, \infty)$. As an example consider a boost in the X^1 - X^{d+1} plane

$$X^1 \cosh \beta = X^{d+1} \sinh \beta \tag{36}$$

for $X^\mu = 0$. Inserting the coordinates into this equation one obtains

$$\tanh \beta = \tanh \beta \sin t. \tag{37}$$

One can see that the trajectory is in fact oscillating with period 2π. For massless particles the trajectory follows $\cosh \rho = \frac{1}{\cos t}$, which implies that for $t = \pm \frac{\pi}{2}$ the particles reach $\rho = \infty$. Therefore, the AdS space can be viewed as a box that confines classical particles.

The duality

The best studied example of the AdS/CFT correspondence is the duality between type IIB string theory on $AdS_5 \times S^5$ and $\mathcal{N} = 4$ $SU(N)$ SYM theory on $S^3 \times \mathbb{R}$. The duality follows from the physics of D3-branes at low energies. To see that, consider N D3-branes in 10-dimensional Minkowski space. The physics of the branes can be viewed in two ways:

- Open string interpretation: D3-branes are higher dimensional submanifolds which open strings can attach to. While the open strings can be described as small excitations of the D3-brane, closed strings can be viewed as excitation of 10-dimensional Minkowski space. The open string interpretation is only trustworthy for $g_s N \geq 1$, when we are able to neglect string interactions. Furthermore, we are only interested in the low energy limit $E\sqrt{l_s} \ll 1$ to which only massless string excitations are contributing. When taking $l_s \to 0$ the closed and open string sectors decouple. The description of the closed strings is then supergravity on 10-dimensional Minkowski-space, whereas open strings on the D3-brane can be described as $\mathcal{N} = 4$ $SU(N)$ SYM.

- Closed string interpretation: D3-branes can be considered as sources for curved backgrounds, on which closed strings can propagate. In order to use that description we need to impose strong coupling $g_s N \to \infty$. The background metric is divided into two regions, either 10-dimensional Minkowski space or $AdS_5 \times S^5$. Going to the low energy limit by taking $l_s \to 0$ again, those two theories decouple. Thus, one obtains supergravity in 10-dimensional space and type IIB string theory on $AdS_5 \times S^5$.

The result are two different description of D3-branes in the low energy limit. Which of them is valid depends on the value of the coupling $g_s N$. Both perspectives conclude in two decoupled descriptions. The open and the closed perspective have to be equivalent as they describe the same physics. Furthermore, both have supergravity on 10-dimensional Minkowski space as one of the decoupled sectors. Therefore, type IIB string theory on $AdS_5 \times S^5$ should be equivalent to $\mathcal{N} = 4$ $SU(N)$ SYM.

Based on that, Maldacena [5] found that

$$g_{YM}^2 = 4\pi g_s \quad \text{and} \quad \frac{R^4}{l_s^4} = g_{YM}^2 N \equiv \lambda \tag{38}$$

where l_s is the string length and R is the curvature of AdS and S. The reliable regime in the gauge theory is the low coupling limit, in which perturbation theory is applicable. Thus, when

$$\lambda = g_{YM}^2 N = 4\pi g_s N = \frac{R^4}{l_s^4} \ll 1, \tag{39}$$

is given. On the other hand, in the opposite case, where $\lambda \gg 1$, the radius R becomes very much smaller than the string length l_s. From the point of view of the strings the space is then approximately flat and the classical gravity description of string theory can be used. It is important to note that for both cases one has to require the string coupling g_s to be small, as we can only use perturbative approaches to string theory. So, while SYM can be used in the weakly coupled limit, classical supergravity can be used in the strongly coupled limit. This makes the duality very useful. However, that fact is exactly the reason why proving this duality is rather difficult. Proving it, would require calculating an observable in both theories, which is generally very challenging. It can be done in a few special cases where it is possible to use different methods, such as integrability, which is reviewed in detail in section 2.3.

One important aspect showing that those theories are the same is to check if they have the same underlying symmetries. As explained in section 2.1, the $\mathcal{N} = 4$ SYM is based on the superconformal group $PSU(2,2|4)$. It can be split into the bosonic part and the fermionic part. The bosonic subgroup is $SU(2,2) \sim SO(4,2)$ and $SU(4) \sim SO(6)$, where the supercharges Q and S are constructing the fermionic part of the supergroup. On the side of the string theory on $AdS_5 \times S^5$, the isometry between AdS_5 and S^5 is given by $SO(4,2)$ and $SO(6)$ which is the same as the bosonic group. Furthermore, one can show that string theory on $AdS_5 \times S^5$ also preserves $PSU(2,2|4)$.

Quantum field theory performed on AdS_{d+1} space works similar to the known theory on flat spacetime. When studying fields in the bulk theory, it has been found that at the boundary of AdS_{d+1} they behave as operators in CFT. Thus, there is a way to define the correlation function of CFT in terms of quantum field theory on an AdS background. This led Witten [6] to formulate

$$\left\langle e^{\int d^d x \phi_0(x)\mathcal{O}(x)} \right\rangle_{\text{CFT}} = Z_{\text{ST}}(\phi_0). \tag{40}$$

The LHS is the generating functional for the source ϕ_0, which is ϕ living on the boundary of AdS. The integral in the exponent should be thought of as a source ϕ_0 that is coupled to a conformal field $\mathcal{O}$. The correlation functions are then derived by

$$\langle \mathcal{O}(p_1) \dots \mathcal{O}(p_n) \rangle = \frac{\delta}{\delta\phi_0(p_1)} \cdots \frac{\delta}{\delta\phi_0(p_n)} \left\langle e^{\int d^4 x \phi_0(x)\mathcal{O}(x)} \right\rangle_{\text{CFT}} \Big|_{\phi_0=0} \tag{41}$$

where p_i are coordinates on the boundary. On the RHS of eq. (40) is the string partition function $Z_{\mathrm{ST}} =$ defined on the boundary. In the classical limit this partition function is $Z \approx e^{-I_S}$ where I_S is the classical supergravity action. A consequence of eq. (40) is that masses of fields on the supergravity side can be related to the dimensions of the operator on the CFT side [6, 40].

2.2.2 Finite temperature: gauge theory

$\mathcal{N} = 4$ SYM, as formulated in section 2.1, does not contain any information regarding temperature dependency. In order to introduce finite temperature to the theory, the time direction can be compactified to a circle with circumference $\beta = 1/T$. Due to conformal invariance, β is not relevant since it can be scaled out [6]. It is only if the spatial directions are compactified as well, that the theory depends non-trivially on the temperature. So by considering $S^1 \times S^3$ we find a phase transition that depends on the ratio $\frac{\beta}{\beta'}$, where β' is the circumference of the spatial dimensions [6]. This compactification can be undone by taking $\beta' \to \infty$ for which $\mathcal{N} = 4$ SYM on $S^1 \times S^3$ reduces to the one on flat space $S^1 \times \mathbb{R}^3$. In SYM on $S^1 \times S^3$ there exist two spin structures that differ in the periodicity of the spinors around the time direction. Thus, one can also find two partition functions

$$Z_1 = (-1)^F \operatorname{Tr} e^{-\beta H} \tag{42}$$

$$Z_2 = \operatorname{Tr} e^{-\beta H} \tag{43}$$

where F is a parameter depending on the boundary conditions of the spinors [6]. The Hamiltonian H describes time propagation in the case where the time direction is $\mathbb{R}$. By looking at a cylinder $\mathbb{R}^1 \times S^3$ as background metric, the Hamiltonian is replaced by the dilatation operator due to the state operator correspondence. The dilation operator does not commute with the supersymmetric operator. Thus, supersymmetry is broken in the finite temperature theory.

The thermodynamic behaviour of the free $\mathcal{N} = 4$ SYM theory is in a confined state for low temperatures, in which only singlets of the constituent particles are found. Whereas for high temperatures those particles are allowed to exists freely. Those two regimes are separated by a phase transition known as the confinement-deconfinement transition at the Hagedorn temperature. By turning on the 't Hooft coupling λ, an intermediate phase establishes. The temperature dependent on the energy can take two different shapes, which are schematically shown in fig. 1. The diagram on the top has

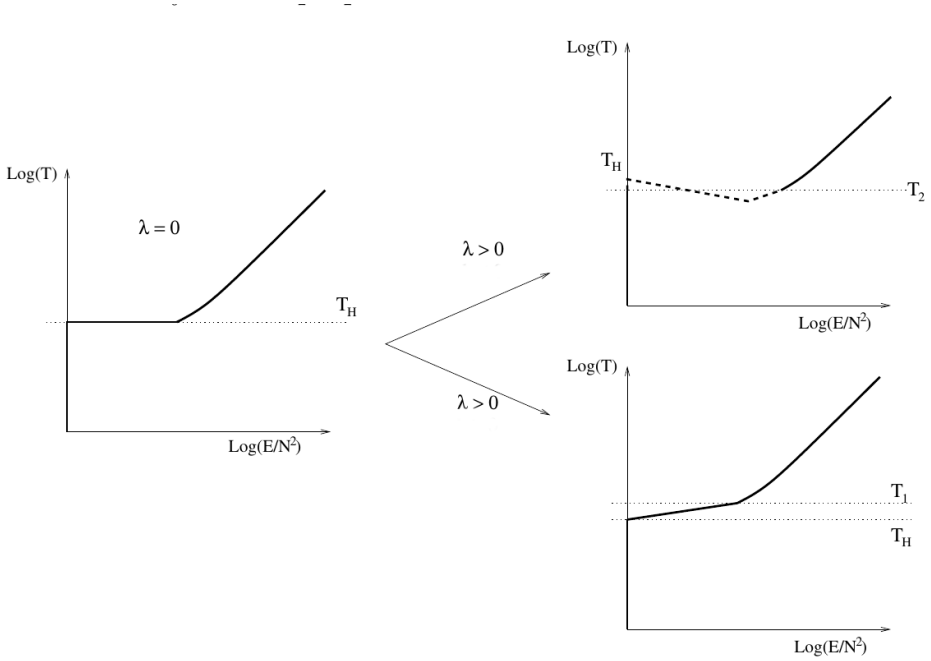

Figure 1: The figure schematically shows the logarithmic temperature T as a function of $\ln\left(\frac{E}{N^2}\right)$. The left diagram is for the free theory $\lambda = 0$, whereas the other two show the dependence for weak coupling $\lambda \ll 1$. The graphic is taken from [15].

a single phase transition at T_2 which is below the Hagedorn temperature T_H, while the diagram on the bottom has two transitions - one at the Hagedorn temperature T_H and another one above [15]. In the following we are going to focus on the top diagram, since it shares the same features as the thermodynamics in string theory.

The thermodynamic behaviour for weakly coupled $SU(N)$ gauge theories can be divided into three different regimes depending on the energy of the system, which are displayed in fig. 2 [15]. The phase for the lowest temperatures is indicated as Phase I in fig. 2. It occurs for temperatures $T < T_1$ and its free energy $F = -\ln(Z)$ (Z is the partition function) scales as N^0. When going to temperatures above T_1, Phase II and Phase III develop. Both have a free energy F that scales as N^2. However, Phase II has a negative free energy and is thus unstable. Thus, only Phase III is accessible at those temperatures. The phase transition between Phase I and Phase III occurs at T_2, which is the confinement-deconfinement phase transition. Above the Hagedorn temperature Phase I disappears and Phase III is the only possible state. For $\lambda = 0$, the Phase II solution does not exist and the confinement-deconfinement transition occurs exactly at the Hagedorn temperature. Furthermore, it is important to note that by taking $N \to \infty$,

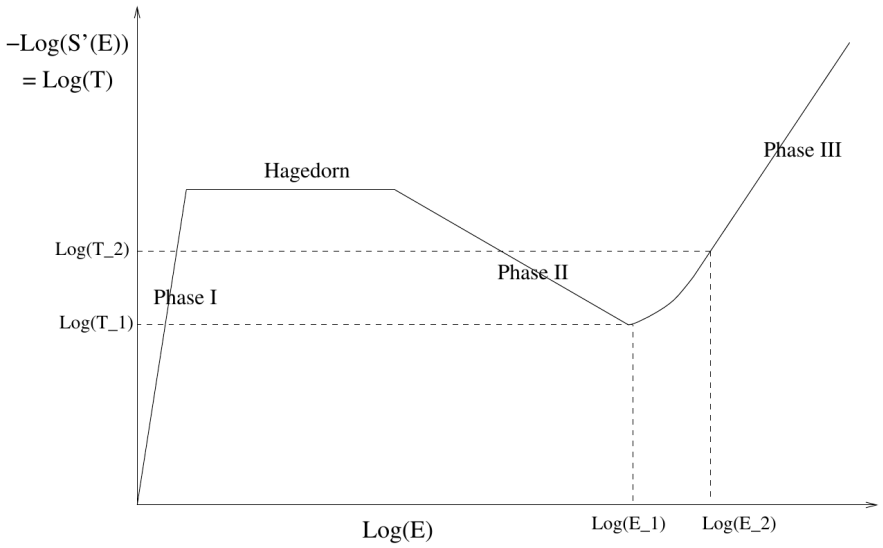

Figure 2: The figure displays a schematic diagram of three different phases in $\mathcal{N} = 4$ SYM as dependency of the logarithmic density of states $S' = \frac{\partial S}{\partial E}$ and temperature T on the logarithmic energy E. This result was found in [15].

all energies after the Hagedorn growth of the density of states are not accessible anymore.

Now we will focus on the high and low temperature regime which are denoted as Phase III and Phase I in fig. 2, respectively. The low temperature is called confined phase. Its most prominent example is found in QCD for temperatures below the confinement-deconfinement temperature. There it becomes manifest in the phenomenon that gluons and quarks can only appear in groups. In non-Abelian gauge theories such as QCD this effect is understood by introducing colours and gluons as colour charge transmitters. This is also the case in more general theories as $SU(N)$ gauge theories on compact manifolds. Gluons and quarks are both particles that carry a colour charge. Thus, by putting a single particle on the manifold Gauss' law would be violated. This means that gluons and quark are only allowed to show up in combinations classified as hadrons and glueballs (only gluons).

In the confined phase, separating two colour charges means that the gluon field builds up a flux tube or an effective string between the charges. Consequently, the potential between the charges grows linearly with the distance L

$$V(L) \approx \sigma L, \quad L \to \infty \tag{44}$$

where σ is the tension of the flux tube. At some point it is energetically favourable to

produce another pair of charges instead of separating the initial charges any further. This leads to the mathematical description of the confinement using the expectation value of Wilson loops [7, 41] over the gauge field A

$$\langle W(C)\rangle = \left\langle \frac{1}{N} \operatorname{tr} P e^{\oint_C A} \right\rangle \sim e^{-L'V(L)}. \tag{45}$$

The last term occurs by taking a rectangular contour with side lengths $L' \to \infty$ and L. Using the AdS/CFT duality one can evaluate that integral and find the corresponding confining potential [42].

This procedure does not work, if we look at finite temperature. However, one can use a similar probe for confinement. Instead of the Wilson loop, we use the expectation value of the Polyakov loop

$$\langle \mathcal{P}\rangle = \frac{1}{N} \operatorname{Tr} P e^{-\oint_{C_x} A}. \tag{46}$$

The Polyakov loop is the integral over a contour C_x around the Euclidean time circle β at some fixed position x. The expectation value of the Polyakov loop is then

$$\langle \mathcal{P}\rangle = e^{-F(T)/T}, \tag{47}$$

where $F(T)$ is the free energy in presence of an external quark. In the confining phase it takes an infinite amount of energy to insert this quark. Therefore, a property of the confining phase is $F(T) \to \infty$ or in terms of the Polyakov loop $\langle \mathcal{P}\rangle = 0$.

Thermodynamically speaking the confined phase is the low temperature limit. The system does not have enough energy yet to allow separate states and the allowed states are gauge-invariant and bound. Thus, this low temperature phase behaves as a gas of glueballs. The free energy of such a model scales as $F(T) \sim N^0$ and all the interacting terms are suppressed by $1/N^2$ [43]. The dominating states have an energy of $E/N^2 \ll 1/R$ and the number of states grows exponentially $\rho \propto e^{E/T_H}$ [15].

When the system reaches the limiting Hagedorn temperature, the particles in their bound states gain enough energy to exist freely. This phase is also called the deconfined state, or quark-gluon plasma in QCD. For infinite space $S^1 \times \mathbb{R}^3$, the entropy for this free gas approximation has been found to be [44]

$$S = \frac{2\pi}{3} N^2 T^3 \tag{48}$$

in the 't Hooft limit. Thus, since $S = -\frac{\partial F}{\partial T}$ holds the free energy F is

$$F = -\frac{\pi^2}{6} N^2 T^4. \tag{49}$$

The free energy has been calculated for strong coupling F_{strong} using the AdS/CFT correspondence [45]. The result shows that the free energy $F_{\text{strong}} = \frac{4}{3} F_{\text{weak}}$, where F_{weak} is the free energy in eq. (49). F_{strong} corresponds to the Bekenstein-Hawking entropy in [45]. One might interpolate between those results for weak ad strong coupling with an ansatz

$$F = -\frac{\pi^2}{6} N^2 T^4 a(\lambda) \tag{50}$$

where $\lim_{\lambda \to 0} a(\lambda) = 1$ and $\lim_{\lambda \to \infty} a(\lambda) = \frac{3}{4}$. However, this interpolation only work when assuming that there is no phase transition as is it the case in flat space. In [7] it was discussed that for finite space $S^1 \times S^3$ the free energy in the high temperature phase still scales as $F \sim N^2$. Therefore, the Polyakov loop defined in eq. (47) has to be finite as well [7].

Phase transition

The low and high temperature limits have distinguished phases that can be identified by certain parameters. One is the expectation value of the Polyakov loop eq. (47). It vanishes in the confined regime and takes finite values at the deconfined phase. Another way to distinguish between the phases is the free energy which jumps from N^0 to N^2 when going from confinement to deconfinement. Thus, the quantity

$$\lim_{N \to \infty} \frac{F(T)}{N^2} \tag{51}$$

can be used as an indicator since it is zero at low temperature and non-zero at high temperatures.

Between those phases there is a phase transition at the limiting temperature called Hagedorn temperature T_H. At that point the confined phase stops existing and for zero-coupling it becomes the transition temperature. In the planar limit, which means $N \to \infty$, it is in general defined as the lowest temperature at which the partition function diverges [46]

$$\lim_{T \to T_H} Z(T) = \infty. \tag{52}$$

The transition is in general not well explored. Its physics depends on the values of the 't Hooft coupling. In free $SU(N)$ gauge theory there exists only one phase transition at T_H of first order which was found by Sundborg in [18]. For $N \to \infty$ the jump from one phase to another is sharp, whereas for finite N this transition starts to smooth out [15]. Considering interactions the behaviour of the phase transition can vary between two options. The first possibility is that there exists a single transition of first order below the critical temperature T_H. In this case the states dominating are growing exponentially with energy. However, the partition function cannot be dominated by highly excited states. The second possibility is that the system undergoes two phase transitions continuously. The first transition is at the Hagedorn temperature and the second is above it. Between those two transitions the system undergoes an intermediate phase. The Hagedorn spectrum is allowed to grow until is reaches the critical temperature. Therefore, singularities are forming in the neighbourhood which indicates a "real" Hagedorn transitions. Which of those two option is selected depends on the field content and the second and third order vacuum loop diagrams [15].

The behaviour of the phase transition is not really known for strong coupling since perturbative approaches do not work. An effective way is offered by lattice or numerical techniques which however have their limitations (see for example [1, 15, 16, 47, 48, 49]). A better method is to exploit the AdS/CFT duality. As already mentioned in section 2.2.1, for strong 't Hooft coupling λ we can use type IIB string theory in the supergravity limit. Therefore, it is possible to use perturbation theory on the gravity side and then relating it back to the dual gauge theory.

2.2.3 Finite temperature: string theory

For the strong 't Hooft coupling we can turn to string theory. The thermodynamic behaviour in type IIB string theory can be found for asymptotically flat space, which is the case when the string length is much smaller than the radius of AdS and S, $l_s \gg R$. Furthermore, we want to be able to apply perturbation theory so we need to take $g_s \to 0$. It has been found that there exist three distinct phases which are dominated by different states (see fig. 3) [24, 50, 51]. The lowest energy regime with $E < E_{\text{Hag}} \sim l_s^{-1}(g_s N)^{9/4}$ is dominated by a gas of supergravity particles on AdS space, which is indicated as "Gravitons" in fig. 3. Its entropy is given as

$$S(E) \sim (ER)^{9/10}. \tag{53}$$

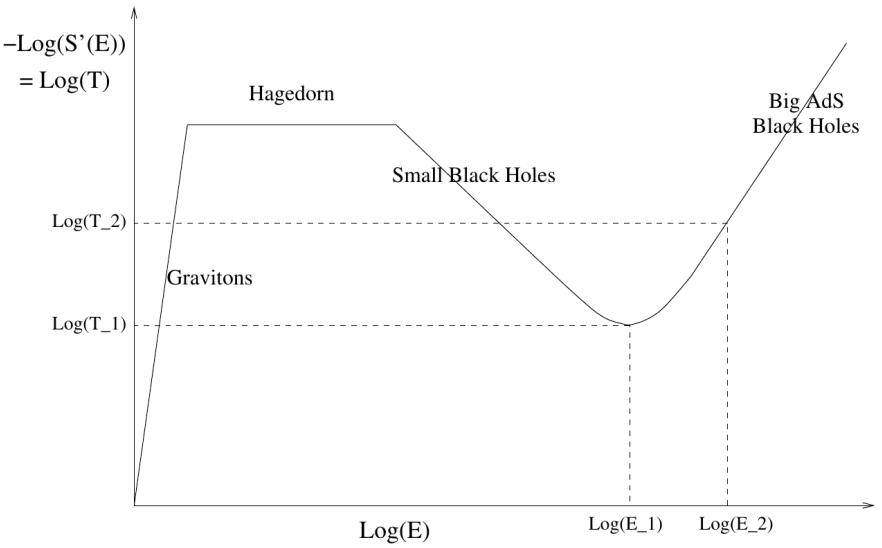

Figure 3: The figure shows schematically the phases of type IIB string theory on the $AdS_5 \times S^5$ background. The logarithmic entropy and the logarithmic temperature are plotted in dependency of the logarithmic energy. This figure is taken from [15].

The second regime is when $E_{\text{Hag}} < E < E_{bh} \sim N^2 R^{-1} (g_s N)^{-7/4}$. The entropy is determined by fundamental strings as is

$$S(E) \sim RE\lambda^{-1/4}. \tag{54}$$

Thus, this is the regime in which the theory displays Hagedorn behaviour. When the energy reaches $E_{bh} < E < E_{\text{AdS}} \sim N^2 R^{-1}$ small black holes start dominating the spectrum. They are formed by free strings that are collapsing. The resulting black holes can then be described by classical supergravity with an entropy of

$$S(E) \sim \left(\frac{l_P E}{R_0}\right)^{8/7} = \left(\frac{E}{N^{1/4}}\right)^{8/7} \tag{55}$$

l_P being the ten-dimensional Planck length. As soon as the energy reaches a certain limit $E > E_{AdS}$ a big black hole is forming. The classical solution is not applicable any more, however, the AdS-Schwarzschild solution is for which the entropy is

$$S \sim N^{1/2} E^{3/4}. \tag{56}$$

Depending on the temperature some of those regimes can be occur and some not. For temperatures below T_1 the on only accessible phase is the gas of supergravity particles. When the temperature reaches T_2, three different regimes can occur, supergravity particles, small black holes or an AdS-black hole (see fig. 3). In order to determine which phase is preferred, one can consider the free energy. This findings show that the

small black hole solution is in fact unstable, as it was the case in section 2.2.2. So, there is a phase transition between the low temperature and high temperature phase which is the Hawking-Page phase transition. The limiting temperature for the transition is the Hagedorn temperature T_H where the low energy regime stops existing. As in section 2.2.2, when taking $N \to \infty$ the small black hole regime and the AdS-black hole regime are not accessible.

Hawing-Page transition

By the Graham-Lee theorem [52], a conformal d-dimensional manifold can be constructed by a summation of Einstein manifolds that induce the conformal manifold at infinity. In our case, the conformal manifold is $S^3 \times S$. Hawking and Page found two Einstein metrics on AdS space that satisfy the theorem [39]. The first metric is known as the thermal AdS metric and is written as

$$ds^2 = \left(\frac{r^2}{R^2} + 1\right) dt^2 + \frac{dr^2}{\left(\frac{r^2}{R^2}\right) + 1} + r^2 d\Omega^2 \tag{57}$$

with the Einstein equations written as

$$R_{ij} = -d\, R^{-2} g_{ij}. \tag{58}$$

R is the radius of curvature of AdS space, $d\Omega$ is the metric of a $(d-1)$-dimensional unit sphere. The time variable t is periodic and, depending on its boundary conditions for fermions, it contributes to either the normal partition function $Z = \mathrm{Tr}\, e^{-\beta H}$ or a partition function taking fermionic boundaries into account $Z = (-1)^F e^{-\beta H}$. The metric can be compactified by introducing points at the boundary $r = \infty$, which means instead of $\mathbb{R}^3 \times S$ we obtain $S^3 \times S$.
The other solution is the Schwarzschild metric for black holes

$$ds^2 = \left(\frac{r^2}{R^2} + 1 - \frac{w_d M}{r^{d-2}}\right) dt^2 + \frac{dr^2}{\frac{r^2}{R^2} + 1 - \frac{w_d M}{r^{d-2}}} + r^2 d\Omega^2 \tag{59}$$

with

$$w_d = \frac{16\pi G_N}{(d-1)\mathrm{Vol}(S^{d-1})}. \tag{60}$$

M is the mass of the black hole and G_N is the $(d+1)$-dimensional Newton constant. The metric has a horizon at

$$\frac{r^2}{R^2} + 1 - \frac{w_d M}{r^{d-2}} = 0. \tag{61}$$

The largest solution of this equation $r = r_+$ gives a singularity which is removed when looking at periodic time coordinates t. The period can be found by requiring smoothness and completeness for the metric

$$\beta_0 = \frac{4\pi R^2 r_+}{d\, r_+^2 + (d-2)R^2}. \tag{62}$$

The period β_0 has a maximum at $r_+ = r_0$ and thus the temperature a minimum at

$$T_0 = \frac{\sqrt{d(d-2)}}{2\pi R^2}. \tag{63}$$

For $T < T_0$ the black hole metric is not defined. Therefore, in the low temperature regime the physics is described on the thermal AdS metric eq. (57). For $T \geq T_0$ both metrics are defined. To determine the dominating metric one can compare the free energy which was done by Hawking and Page in [39]. They concluded that for $r_+ < R$ the thermal AdS metric dominates whereas for $r_+ > R$ the black hole solution takes over. At the limit $r_+ = R$ there is a phase transition which is called the Hawking-Page transition and the corresponding temperature is

$$T = \frac{d-1}{2\pi L}. \tag{64}$$

2.2.4 Phase transition comparison

In terms of the AdS/CFT correspondence the phase transition found in the gauge theory and in the string theory should be the same. This was already suspected by Witten in [6, 7]. One of the findings in [15] has been that the density of states for weak coupling (see fig. 2) has a similar energy dependence as the one found in string theory (see fig. 3). Both theories have three phases for which the scaling of the entropy is the same. Further, at the Hagedorn temperature they both display Hagedorn behaviour. This is a very reassuring argument that the transitions are in fact connected by the AdS/CFT correspondence. However, for weak coupling the phase transition in the gauge theory undergoes an intermediate phase (Phase II in fig. 2) [15]. In terms of the string theory, the corresponding phase would be dominated by small black holes (see fig. 3) that have to be stable. Such small stable black holes have been found later by Berenstein [53].

2.2.5 Hagedorn temperature

The Hagedorn temperature is a limiting temperature for exponentially growing density of states $\rho(E)$ [46] and a partition function of the form

$$Z(T) = \sum_E \rho(E) e^{-\frac{E}{T}}. \tag{65}$$

In the free theory the phase transition is at the Hagedorn temperature and the confined phase stops existing. As mentioned in section 2.2.2 introducing coupling the phase transition already occurs below the Hagedorn temperature. The indicator of this critical point is the partition function which diverges at this temperature

$$\lim_{T \to T_H} Z(T) = \infty. \tag{66}$$

Since we do not consider chemical potentials the partition function is the canonical partition function $Z(T) = \sum_i e^{-E_i/T}$. In order to find the expression for $Z(T)$ one has to determine the contributing states which is normally a formidable task. As an example, in the following the canonical partition function for the free theory is reviewed following [18] and [15].

The free theory can be described as a system of decoupled harmonic oscillators on $S^3 \times S^1$. They are located on a sphere and thus have infinitely many degrees of freedom. The bound states constituting hadrons are represented as single trace states (see section 2.1.2). The other contributing states are multi-trace states. In order to count the relevant states one has to consider two important facts. First, due to the constituent traces the states are invariant under cyclic permutations. Second, in $SU(N)$ groups there arise relations among traces. The number of such relations depends on the value of N. Fortunately, in the limit $N \to \infty$ there remain no trace relations which simplifies the counting process tremendously. Taking everything in consideration the number of constituent states can be found counting the non-cyclic combinations of ordering the fields inside the trace. One can use Pòlya's theorem [54] to do that.

In general the single-site partition functions for bosons and fermions are defined as

$$z_B(\beta) = \sum_{n=1} e^{-\beta E_{B,n}}, \quad z_F(\beta) = \sum_{n=1} e^{-\beta E_{F,n}}. \tag{67}$$

In the following we will use the notation $x \equiv e^{-\beta} \equiv e^{-\frac{1}{T}}$. One may observe that each $z(x) = \sum_i x^{E_i}$ has a unique solution for $z(x) = 1$ at $x = x_H = e^{-1/T_H}$ and $0 < x < 1$.

Since all the states are in the adjoint representation of $SU(N)$ they are all one or more traces.
In the planar limit the scaling dimensions of the multi trace operators are all determined by single trace operators [18].

It is convenient to first find a upper limit for the partition function of all single trace operator. Say we have a number of k fields inside each trace then one can write a first expression for the partition function

$$Z_{ST} = \sum_{k=1}^{\infty} \frac{z(x)^k}{k} + f(k) = -\ln(1 - z(x)) + f(k). \tag{68}$$

The factor of $\frac{1}{k}$ reduces the number of states by their cyclicity. The function $f(k)$ accounts for all the states that should not be considered. The contributing states could for example be reduced by general repetitions of the fields inside the trace. By using Pòlya's theory one can also take those repetitions into account and find an exact expression for the large N limit [15]

$$Z_{ST} = -\sum_{k=1}^{\infty} \frac{\varphi(k)}{k} \ln\Big(1 - z(x^k)\Big). \tag{69}$$

Here we introduced the Euler totient function $\varphi(k)$ that gives the number of positive integers that are less than k and relatively prime to k [18].
Now we have to sum over all states that with arbitrary many traces and obtain [15]

$$\ln(Z) = \sum_{n=1}^{\infty} \frac{1}{n} Z_{ST}(x^n) = -\sum_{k=1}^{\infty} \ln\Big(1 - z(x^k)\Big) = -\sum_{k=1}^{\infty} \ln\Big(1 - z_B(x^k) + (-1)^k z_F(x^k)\Big). \tag{70}$$

This is only valid for $N \to \infty$ because otherwise trace relations would have to be considered in the counting. Remember that we defined $z(x_H) = 1$, then Z is well defined for $\beta > \beta_H$ and diverges as $-\ln(\beta - \beta_H)$ for $\beta \to \beta_H$. However, eq. (70) is ill-defined for $\beta < \beta_H$. Thus, the divergence shows that T_H is the limiting temperature for $N \to \infty$ [15].

A more specific condition for eq. (70) to be valid, is that the length of the single trace operators has to be much smaller than N^2 [15]. This is a problem for finite N theories but is also states a problem for temperatures $T > T_H$, since it is ill defined there. Using a more advanced logic a matrix model has been found that allows an exact solution for the partition function [15].

To find the Hagedorn temperature for the free theory it is in fact enough to state the condition that the single partition function $z(x_H) = z_B(x_H) + z_F(x_H) = 1$. It turns

out that for $\mathcal{N}=4$ SYM on $S^3 \times \mathbb{R}$

$$z_B(x) = \frac{6x + 12x^2 - 2x^3}{(1-x)^3} \tag{71}$$

$$z_F(x) = \frac{16x^{3/2}}{(1-x)^3}. \tag{72}$$

The Hagedorn temperature per unit of the radius R for the free SYM theory is thus given as

$$T_H = -\frac{1}{\ln(x_H)} = -\frac{1}{\ln\left(7-4\sqrt{3}\right)} \simeq 0.379663. \tag{73}$$

In the following we look at the partition function for the free theory and how the Hagedorn temperature can be obtained by it. It is also possible to find the Hagedorn temperature for weak coupling by using a perturbative approach. In [15] Aharony, Marsano, Minwalla, Papadodimas and van Raamsdonk work with a matrix model that can be used for weak coupling. However, going to strong coupling is not possible with such methods. One way to solve this is to use numerical extrapolation methods, which was also performed in [15], or one can use certain lattice techniques. Another way to solve this problem is using integrability of $\mathcal{N}=4$ SYM, which will be reviewed in section 2.3. After introducing that property we will review a method in section 2.3.5 to find the Hagedorn temperature using the partition function as it was done by Harmark and Wilhelm in [55].

2.3 Integrability and quantum spectral curves

Integrability is a property of planar $\mathcal{N}=4$ SYM and free type IIB string theory on $AdS_5 \times S^5$ that allows an exact solution for some physical quantities, including thermodynamics. On the string theory side, integrability occurs naturally [20]. The strings on $AdS_5 \times S^5$ can be described by a non-linear two-dimensional sigma model [56]. For such a theory there exists a non-Abelian Lax-connection. To obtain integrability it is required that the curvature of the Lax-connection vanishes (see e.g. [20, 57]). This then provides a description of the spectra of the algebraic curves (see for example [58, 59, 60] for a review). It has been found that the spectra exactly match the ones of $\mathcal{N}=4$ SYM [61].

On the gauge theory side, integrability occurs by identifying the anomalous dimension operator with the Hamiltonian of a spin chain which are known to be solved by the Bethe ansatz (BA) or the thermodynamic Bethe ansatz (TBA) [62, 63, 64]. The TBA contains a set of non-linear integral equations that can be formulated as what is known

as Y-system [62, 65]. It is a system of infinite finite-difference equations and is further related to the T-system [62] which is integrable. Therefore, it is possible to reduce the T-system to a finite set of equations which is known as Q-system or quantum spectral curve (QSC). The constituent Q-function depend on the spectral parameter and are related to Baxter polynomials of a spin chain [66]. How this spin chain establishes from planar $\mathbf{N} = 4$ SYM is going to be reviewed in this section following closely [67]. In the end we are going to explain how this approach can be applied to the solution of the Hagedorn temperature using the methods in [1].

2.3.1 QSC for $SU(2)$

To get an understanding of how the spin chain manifests in SYM we will first study the $SU(2)$ sector. There, the operators are two complex scalar fields $X = \phi^1 + i\phi^4$ and $Y = \phi^2 + i\phi^5$. Furthermore, the sector is closed which means that the operator mixing also stays in this sector, making the description very convenient.
As already established in section 2.1.4, considering quantum corrections changes the scaling dimension of operators (except if they are protected). One can find a corresponding operator that has the anomalous dimension as an eigenvalue. This operator was defined in eq. (24). The trace operator K vanishes within Γ as we consider the case of the closed $SU(2)$ sector. Thus, the expression eq. (24) reduces to

$$H = 2g^2 \sum_{l=1}^{L} (1 - P_{l,l+1}), \tag{74}$$

where we introduced the effective planar coupling $g^2 = \frac{\lambda}{16\pi^2}$. However, this is in fact the Hamiltonian of an $SU(2)$ Heisenberg spin chain. One can identify $P_{l,l+1}$ with spin operators $\vec{S}$ such that the operator Γ reads as the well known Hamiltonian for the spin chain

$$H_{\text{spinchain}} = 2g^2 \sum_{l=1}^{L} (1 - \vec{S}_l \cdot \vec{S}_{l+1}) \tag{75}$$

The spin chain described by eq. (74) with L spin sites. Furthermore, the operator only affects the l and $l+1$ site which means that the interaction between the spins is restricted to the nearest neighbour [19]. Since we are in the $SU(2)$ sector, only two independent states are allowed for eq. (74). Using the spin chain analogy we can identify them with spin up and spin down state. The ground state is then defined as the state where all spins are aligned in the same direction. The total spin is $L/2$ for that case. Furthermore,

one can set boundary conditions for the chain for instance twisted boundaries which are defined as

$$\begin{aligned} P_{L,L+1} \left|\uparrow \dots \uparrow\right\rangle &= \left|\uparrow \dots \uparrow\right\rangle, \\ P_{L,L+1} \left|\downarrow \dots \downarrow\right\rangle &= \left|\downarrow \dots \downarrow\right\rangle, \\ P_{L,L+1} \left|\downarrow \dots \uparrow\right\rangle &= e^{-2i\phi} \left|\uparrow \dots \downarrow\right\rangle, \\ P_{L,L+1} \left|\uparrow \dots \downarrow\right\rangle &= e^{2i\phi} \left|\downarrow \dots \uparrow\right\rangle. \end{aligned} \tag{76}$$

Excitations in spin chains can propagate through the chain with a momentum p_i and behave as quasi-particles which are called magnons. One can introduce the rapidity variable u_i which relates to the momentum as

$$e^{ip_i} = \frac{u_i + i/2}{u_i - i/2}. \tag{77}$$

An ansatz to find the eigenvalues and eigenvectors for the Heisenberg spin chain was derived first by Bethe in [68]. If there are two excited states with momenta u_i and u_k right next to each other they scatter and pick up a phase

$$\Phi(u_i, u_k) = 2 \arctan(u_i - u_k). \tag{78}$$

The process is described more generally by introducing a scattering matrix

$$S_{ik} = \frac{u_i - u_k - i}{u_i - u_k + i}. \tag{79}$$

Together with the boundary conditions one can find a set of equations

$$\left(\frac{u_k + i/2}{u_k - i/2}\right)^L = e^{-2i\phi} \prod_{j \neq k}^{N} \frac{u_k - u_j + i}{u_k - u_j - i}, \tag{80}$$

where $k = 1 \dots N$. They are called Bethe equations and are generally used to describe the spectral problem of spin chains. Equation (80) is for the $SU(2)$ case but they have been generalized to other spin chains (see for example [69, 70]).

The energy spectrum of the spin chain which contains N magnons is found to be

$$E = \sum_{i=1}^{N} \frac{2g^2}{u_i^2 + 1/4} \tag{81}$$

and the corresponding state of the spin chain can be described in form of Baxter Q-functions (introduced by Baxter in [71])

$$Q_1(u) = e^{\phi u} \prod_{i=1}^{N_1} (u - u_{1,i}). \tag{82}$$

Equation (82) depends on the parameter u which is the spectral parameter and this equation also contains a product of N_1 Bethe-roots u_i. The function $Q_1(u)$ describes a spin up particle propagating in a sea of spin down particles or vice versa. Thus, if we have N_1 particles with spin up propagating through the chain, we obtain a polynomial of order N_1. Consequently, there must exist a dual polynomial of order $N_2 = L - N_1 + 1$ that describes the spin down particles instead of spin up. So we have the two solutions [72]

$$Q_1(u) = e^{\phi u} \prod_{i=1}^{N_1} (u - u_{1,i}), \quad Q_2(u) = const \times e^{-\phi u} \prod_{i=1}^{L-N_1+1} (u - u_{2,i}). \tag{83}$$

One can rewrite the energy spectrum eq. (81) in a more general way using the Q-function

$$E = i\partial_u \log \frac{Q_1^+}{Q_1^-}\bigg|_{u=0}, \tag{84}$$

where we introduced the convenient notation $f^{[\pm a]} = f(u \pm ia/2)$ and $f^{[\pm 1]} = f^{\pm}$.

The Baxter equation in the $SU(2)$ case is found to be [73]

$$TQ = Q^{++} \left(u - \frac{i}{2}\right)^L + Q^{--} \left(u + \frac{i}{2}\right)^L, \quad T(u) = \begin{vmatrix} Q_1^{++} & Q_1^{--} \\ Q_2^{++} & Q_2^{--} \end{vmatrix} \tag{85}$$

where Q is a generic polynomial. The functions $Q_1(u)$ and $Q_2(u)$ are two linear independent solutions of the Baxter equation eq. (85). Thus, a new Q-function can be constructed up to a constant by

$$\begin{vmatrix} Q_1^- & Q_1^+ \\ Q_2^- & Q_2^+ \end{vmatrix} = const \cdot Q_{12} Q_\emptyset. \tag{86}$$

The function is found to be $Q_{12}(u) \propto u^L$ while $Q_\emptyset = 1$ is introduced for later convenience. The function $Q_\emptyset$ can be interpreted as a boundary function as it depends on the specific underlying model. The numeric constant is not important for the relations now since it can be found by looking a the large u limit. Equation (86) combined it with the Baxter equation eq. (85) it can be written as

$$D(u) = \begin{vmatrix} Q^{++} & Q & Q^{--} \\ Q_1^{++} & Q_1 & Q_1^{--} \\ Q_2^{++} & Q_2 & Q_2^{--} \end{vmatrix} = 0. \tag{87}$$

Since $T(u)$ is in general unknown eq. (87) can be used to determine $T(u)$. To do so an additional information on the structure of $T(u)$ is needed. In case of the $SU(2)$ it is

enough to require polynomiality for T. Equation (86) is known as the QQ-relation for the $SU(2)$ algebra and is the main ingredient for the QSC [67].

To summarize, the spectral problem of the spin chain is described by Q-functions which depend on the spectral parameter u. They satisfy the Baxter equation and thus the Bethe equations. In addition to the relations between the functions one also needs to know the analytic properties of the functions. This approach can be generalized to other algebras where the relations and the functions become more evolved, however, the main concept stays the same.

2.3.2 QSC for $PSU(2,2|4)$

In this section we will discuss the principles introduced in section 2.3.1 for $\mathcal{N}=4$ SYM. The underlying symmetry of the theory is $PSU(2,2|4)$. However, this is just $SU(4|4)$ with a projection and real form. Thus, we can just use $SU(4|4)$ for the QQ-relation in $\mathcal{N}=4$ SYM. In the following we will refer to $SU(4)$ and its supersymmetric part as bosonic and fermionic part, respectively.

Bosonic QQ-relations

First, we are going to focus on the bosonic part separately which is possible since the structure does not change by including supersymmetry in the problem. The QQ-relation in eq. (86) can be even more generalized to any $SU(N)$ algebra [73]

$$\begin{vmatrix} Q^-_{Ab} & Q^+_{Ab} \\ Q^-_{Ac} & Q^+_{Ac} \end{vmatrix} \propto Q_A Q_{Abc} \tag{88}$$

or in the more convenient form

$$Q_A Q_{Abc} = Q^+_{Ab} Q^-_{Ac} - Q^-_{Ab} Q^+_{Ac}. \tag{89}$$

The indices $b,c = 1,2\ldots,N$ and A is a multi-index which can take on any single indices,no index, any combination of indices or all indices. For instance, by identifying $I=\emptyset$, and $b,c=\{1,2\}$ eq. (88) reduces to eq. (86). This relation is very powerful since one can construct any function $Q_{ij\ldots k}$ out of it by applying it successively. It is important to note, however, that the order of the indices in A does matter as $Q_{12} = -Q_{12}$. Therefore, the multi-index will be defined as sorted $A = a_1, a_2 \ldots, a_N$ for $a_k < a_{k+1}$. Thus, one can find a set of Q-functions using the QQ-relation eq. (89) which are all

solution to the Bethe equations. Since they are all independent solutions they should satisfy the Baxter equation

$$\begin{vmatrix} Q & Q^{[2]} & \cdots & Q^{[2n]} \\ Q_1 & Q_1^{[2]} & \cdots & Q_1^{[2n]} \\ \vdots & \vdots & \ddots & \vdots \\ Q_N & Q_N^{[2]} & \cdots & Q_N^{[2n]} \end{vmatrix} = 0. \tag{90}$$

The Q-functions all have a Hodge dual defined as

$$Q_A = \epsilon_{A\bar{A}} Q^{\bar{A}}, \tag{91}$$

where $\epsilon_{1,2\ldots N} = \epsilon^{1,2\ldots N} = 1$. The index A is a multi-index and $\bar{A}$ is a multi-index of the set $\{\bar{A}\} = \{1, 2 \ldots N\}/\{A\}$. Note, that there is no summation over the indices.

The Q-functions are in fact depend on the gauge while the Y-system is independent under rescalings of the form

$$Q_A \mapsto g_{(+)}^{[|A|]} g_{(-)}^{[-|A|]} Q_A. \tag{92}$$

The functions $g_{(\pm)}$ are arbitrary functions of u and can be interpreted as local gauge transformations. The Q-functions are nonetheless invariant under rotations also called H-symmetry [21]

$$\tilde{Q}_{b_1 b_2 \ldots b_n} \mapsto \sum_{c_1, c_2, \ldots c_n \in \mathcal{B}} h_{b_1 c_1}^{[n-1]} h_{b_2 c_2}^{[n-1]} \ldots h_{b_n c_n}^{[n-1]} Q_{c_1 c_2 \ldots c_n}, \quad \mathcal{B} = \{1, 2 \ldots N\}. \tag{93}$$

h_{bc} are i-periodic functions of the spectral parameter u for which $h^+ = h^-$.

Fermionic QQ-relations

Introducing supersymmetry to the relations above can be accomplished by simply relabelling the Q-functions. More specifically if we rename the bosonic Q-functions $Q_A \to \mathcal{Q}_A$, the fermionic functions can then be found by

$$Q_{A|I} = \epsilon^{\bar{I}I} \mathcal{Q}_{A(\bar{I}+M)}. \tag{94}$$

First, it is important to note, that there is no actual summation over the index $\bar{I}$. Furthermore, here A and I are both multi-indices in the sets $\{1, \ldots N\}$ and $\{1, \ldots M\}$ respectively. The index $\bar{I}$ is defined as $\bar{I} = \{1, \ldots, N\}/I$. Also, $(\bar{I} + M)$ means that to each element of the set $\bar{I}$ we add M. We will address the index A as the bosonic and

I as the fermionic part of the function. For the case of $\mathcal{N}=4$ SYM N and M both become four.

Instead of one QQ-relation eq. (89) there are now three relations [66, 74]

$$Q_{A|I}Q_{Aab|I} = Q^{+}_{Aa|I}Q^{-}_{Ab|I} - Q^{-}_{Aa|I}Q^{+}_{Ab|I}\,, \tag{95}$$

$$Q_{A|I}Q_{A|Iij} = Q^{+}_{A|Ii}Q^{-}_{A|Ij} - Q^{-}_{A|Ii}Q^{+}_{A|Ij}\,, \tag{96}$$

$$Q_{Aa|I}Q_{A|Ii} = Q^{+}_{Aa|Ii}Q^{-}_{A|I} - Q^{-}_{Aa|Ii}Q^{+}_{A|I}\,. \tag{97}$$

The first one is just the bosonic relation eq. (89) and the other two connect the fermionic parts of the Q-function. Additionally, one has the freedom to choose the boundary functions which are in this work going ot be $Q_{\emptyset|\emptyset}=1$ and $Q_{12\ldots N|12\ldots M}=1$. All the Q-functions satisfy the Bethe equations [74]

$$-1 = \frac{Q_{A|I}(u+i/2)\,Q_{Aa|I}(u-i)\,Q_{Aab|I}(u+i/2)}{Q_{A|I}(u-i/2)\,Q_{Aa|I}(u+i)\,Q_{Aab|I}(u-i/2)} \qquad \text{for } u=u_{Aa|I}, \tag{98}$$

$$-1 = \frac{Q_{A|I}(u+i/2)\,Q_{A|Ii}(u-i)\,Q_{A|Iij}(u+i/2)}{Q_{A|I}(u-i/2)\,Q_{A|Ii}(u+i/2)\,Q_{A|Iij}(u-i/2)} \qquad \text{for } u=u_{A|Ii}, \tag{99}$$

$$1 = \frac{Q_{Aa|Ii}(u+i/2)\,Q_{A|I}(u-i/2)}{Q_{A|I}(u+i/2)\,Q_{Aa|Ii}(u-i/2)} \qquad \text{for } u=u_{Aa|i} \text{ or } u=u_{A|Ii}, \tag{100}$$

where $u_{Aa|I}$ is a root of the function $Q_{Aa|I}(u)$ and $u_{A|Ii}$ of $Q_{A|Ii}$. However, there are only a few fundamental Q-function of which all others can be constructed out of using eqs. (95) to (97). The basic elements are $\mathbf{P}_a = Q_{a|\emptyset}$ and $\mathbf{Q}_i = Q_{\emptyset|i}$ where $a=1,2,\ldots N$ and $i=1,2,\ldots M$. A semi-fundamental function which is also going to be important in the following is $Q_{a|i}(u)$. Inserting $I, A=\emptyset$ in eq. (97) it reduces to the following equation depending only on the elementary Q-functions

$$\mathbf{P}_a\mathbf{Q}_i = Q^{+}_{a|i} - Q^{-}_{a|i}. \tag{101}$$

Starting from this equation it is possible to reconstruct Q-functions with more bosonic indices. As an example consider $A=\emptyset$ and $I=i$ from eq. (95) one can obtain Q-functions with more bosonic indices

$$Q_{ab|i} = \frac{Q^{+}_{a|i}Q^{-}_{b|i} - Q^{-}_{a|i}Q^{+}_{b|i}}{\mathbf{Q}_i}. \tag{102}$$

The same works for the fermionic index using eq. (96). Therefore, it is sufficient to only consider the fundamental function $\mathbf{P}_a$ and $\mathbf{Q}_i$. The Baxter equation of the Q-system can also be expressed as a function only depending on $\mathbf{P}_a(u)$

$$\begin{aligned} 0 = D_0\mathbf{Q}^{[+4]} - \mathbf{Q}^{[+2]}\left(D_1 - \mathbf{P}^{[+2]}_a\mathbf{P}^{a[+4]}D_0\right) \\ + \frac{1}{2}\mathbf{Q}\left(D_2 - \mathbf{P}_a\mathbf{P}^{a[+2]}D_1 + \mathbf{P}_a\mathbf{P}^{a[+4]}D_0\right) + c.c. \end{aligned} \tag{103}$$

where $\mathbf{Q}$ has four solutions which correspond to $\mathbf{Q}_i(u)$ and the coefficients are

$$
\begin{aligned}
D_0 &= \det \begin{pmatrix} \mathbf{P}^{1[+2]} & \mathbf{P}^{2[+2]} & \mathbf{P}^{3[+2]} & \mathbf{P}^{4[+2]} \\ \mathbf{P}^{1} & \mathbf{P}^{2} & \mathbf{P}^{3} & \mathbf{P}^{4} \\ \mathbf{P}^{1[-2]} & \mathbf{P}^{2[-2]} & \mathbf{P}^{3[-2]} & \mathbf{P}^{4[-2]} \\ \mathbf{P}^{1[-4]} & \mathbf{P}^{2[-4]} & \mathbf{P}^{3[-4]} & \mathbf{P}^{4[-4]} \end{pmatrix}, \\
D_1 &= \det \begin{pmatrix} \mathbf{P}^{1[+4]} & \mathbf{P}^{2[+4]} & \mathbf{P}^{3[+4]} & \mathbf{P}^{4[+4]} \\ \mathbf{P}^{1} & \mathbf{P}^{2} & \mathbf{P}^{3} & \mathbf{P}^{4} \\ \mathbf{P}^{1[-2]} & \mathbf{P}^{2[-2]} & \mathbf{P}^{3[-2]} & \mathbf{P}^{4[-2]} \\ \mathbf{P}^{1[-4]} & \mathbf{P}^{2[-4]} & \mathbf{P}^{3[-4]} & \mathbf{P}^{4[-4]} \end{pmatrix}, \\
D_2 &= \det \begin{pmatrix} \mathbf{P}^{1[+4]} & \mathbf{P}^{2[+4]} & \mathbf{P}^{3[+4]} & \mathbf{P}^{4[+4]} \\ \mathbf{P}^{1[+2]} & \mathbf{P}^{2[+2]} & \mathbf{P}^{3[+2]} & \mathbf{P}^{4[+2]} \\ \mathbf{P}^{1[-2]} & \mathbf{P}^{2[-2]} & \mathbf{P}^{3[-2]} & \mathbf{P}^{4[-2]} \\ \mathbf{P}^{1[-4]} & \mathbf{P}^{2[-4]} & \mathbf{P}^{3[-4]} & \mathbf{P}^{4[-4]} \end{pmatrix}.
\end{aligned}
\tag{104}
$$

The symmetries of the Q-functions of $SU(N|M)$ are similar to their bosonic analogue eqs. (92) and (93). The functions are invariant under gauge transformations

$$
Q_{A|I} \mapsto g_1^{[|A|-|I|]} g_2^{[-|A|+|I|]} Q_{A|I} \tag{105}
$$

instead of rescaling invariance. The other symmetry is H-symmetry which affects the Q-functions as

$$
Q_{A|I} \mapsto \sum_{|B|=|A|,\,|J|=|I|} \left(H_b^{[|A|-|I|]}\right)_A^B \left(H_f^{[|A|-|J|]}\right)_I^J Q_{B|J}, \tag{106}
$$

where H are i-periodic and arbitrary functions.

Furthermore, one can also define Hodge duals to the Q-functions

$$
Q^{A|I} = (-1)^{|A||I|} \epsilon^{\bar{A}A} \epsilon^{\bar{I}I} Q_{\bar{A}\bar{I}} \tag{107}
$$

where there is no summation over the indices and $\{\bar{A}\} = \{1, 2, \dots N\}/\{A\}$ and $\{\bar{I}\} = \{1, 2, \dots M\}/\{I\}$. They satisfy the same QQ-relations as the usual Q-relations. In addition, one can choose freely the form of $Q_{\emptyset|\emptyset} = 1$ since it can be used as the normalization. Furthermore, we can also specify $Q_{1234|124} = Q^{\emptyset|\emptyset} = 1$. This is rather non-trivial and can be seen as the uni-modularity which is needed to obtain $PSU(2,2|4)$ from $SU(2,2|4)$. With the definition fo the Hodge dual it is possible to find some relevant properties for

the basic Q-functions

$$\mathbf{Q}_i \mathbf{P}_a Q^{a|i} = 0, \tag{108}$$

$$\mathbf{P}_a \mathbf{P}^a = \mathbf{Q}_i \mathbf{Q}^i = 0, \tag{109}$$

$$Q_{a|i} Q^{b|i} = \delta_a^b, \tag{110}$$

$$Q_{a|i} Q^{a|j} = \delta_i^j. \tag{111}$$

In the $SU(2)$ case, we mentioned that only knowing the QQ-relations is not enough. To fully determine all the Q-function some information about their structure is needed. For the $SU(2)$ Heisenberg spin chain one could make the assumption that all Q-functions are simply polynomials. However, this is in general not the case for other set ups. To find the form of the Q-functions one needs to consider boundary conditions and their analytic properties.

2.3.3 Analytic properties

The QQ-relations make up a finite difference system of equations that reflect the $PSU(2,2|4)$ symmetry. We already mentioned in sections 2.3.1 and 2.3.2 that to describe the QSC one has to know the QQ-relations and their analytic properties. For spin chains the Q-functions are usually polynomials, however, this is not the case in general. As will be discussed here, introducing boundary conditions breaks this condition. Furthermore, the objective is to find a description of the thermodynamics in terms of the coupling. But to this point neither any of the functions nor any of the equations contain any dependency of the 't Hooft coupling. In fact, we can include this information by finding additional analytical properties for the Q-functions which depend on the specific physics of the observable.

We are interested in the thermodynamic properties of the spin chain where the free energy is of special interest. To calculate the free energy one has two important parameters, the temperature T and the length of the spin chain L. The QSC considered so far has been derived at zero temperature and had a finite length L. In geometric terms that can be interpreted as a theory on a torus with circumferences L and $\beta = 1/T$. Taking $T \to 0$ the circumference $\beta \to \infty$ and thus the torus becomes a cylinder with infinite length and finite circumference L. To find the Hagedorn temperature the QSC should be considered for finite β as well as finite L which however is not been solved yet. Nonetheless, since we are only interested in the Hagedorn temperature we can make some simplifications [55]. Near the Hagedorn singularity the dominating states all have

very high energies which means high scaling dimensions D and further high lengths of the spin chain L [55]. Thus, one can say that the Hagedorn QSC is defined on a cylinder with finite circumference β and infinite length L. Or rather by taking the scaling dimension $D \to \infty$ [55].

The two theories can be converted into each other by performing a double Wick rotation and therefore they differ in some properties. One main difference is the analytic structure of the Q-functions. We are going to see later that the Q-functions have either long or short branch cuts. The double Wick rotation converts the form of the branch cuts from QSC into the opposite in Hagedorn QSC. Another difference is the boundary conditions for the periodicity of the spin chain. In the Hagedorn QSC those become twisted boundary conditions [55]. The twist enters the problem as a deformation of the Bethe equations eqs. (98) to (100). The constants -1 or 1 on the left hand side of eqs. (98) to (100) are now replaced by twist variables x_a, y_i

$$-\frac{x_b}{x_a} = \frac{Q_{A|I}(u+i/2)\, Q_{Aa|I}(u-i)\, Q_{Aab|I}(u+i/2)}{Q_{A|I}(u-i/2)\, Q_{Aa|I}(u+i)\, Q_{Aab|I}(u-i/2)} \qquad \text{for } u = u_{Aa|I}, \tag{112}$$

$$-\frac{y_j}{y_i} = \frac{Q_{A|I}(u+i/2)\, Q_{A|Ii}(u-i)\, Q_{A|Iij}(u+i/2)}{Q_{A|I}(u-i/2)\, Q_{A|Ii}(u+i/2)\, Q_{A|Iij}(u-i/2)} \qquad \text{for } u = u_{A|Ii}, \tag{113}$$

$$\frac{x_a}{y_i} = \frac{Q_{Aa|Ii}(u+i/2)\, Q_{A|I}(u-i/2)}{Q_{A|I}(u+i/2)\, Q_{Aa|Ii}(u-i/2)} \qquad \text{for } u = u_{Aa|i} \text{ or } u = u_{A|Ii}. \tag{114}$$

One can approach the spectral problem in two ways. The first method is to work with the deformed Bethe equations and adapt the QQ-relation to the deformed problem. The second possibility is to introduce an exponential prefactor to the Q-functions

$$\left(\frac{\prod_a x_a}{\prod_i y_i}\right)^{-iu}. \tag{115}$$

This however breaks the polynomiality of the Q-functions that has been assumed until now [75]. In the following we are going to use the exponential prefactor.

Asymptotic limit

In the asymptotic limit for large spectral parameter u the Q-functions reduce to simple functions that are determined by the charges of $PSU(2,2|4)$ [73]. Hence, the analytic structure of the Q-functions is easily accessible in this limit. Harmark and Wilhelm [1, 55] derived the large u limit using the TBA for the Hagedorn QSC. They found that the Q-functions need to have Cartan charges $(S_1, S_2, J_1, J_2, J_3) = (0, 0, 0, 0, 0)$ to match the calculated T-system. Furthermore, the scaling dimension is kept fixed in

the calculation in [55]. Thus, the Hagedorn temperature is then only determined by changing the twists. This was done using the T-system in [55] and they found

$$\begin{aligned}
\mathbf{P}_1(u) &= A_1 \left(-e^{-\frac{1}{2T_H}}\right)^{-iu} \left(1+\mathcal{O}(u^{-1})\right), \\
\mathbf{P}_2(u) &= A_2 \left(-e^{-\frac{1}{2T_H}}\right)^{-iu} \left(u+\mathcal{O}(u^{0})\right), \\
\mathbf{P}_3(u) &= A_3 \left(-e^{-\frac{1}{2T_H}}\right)^{+iu} \left(1+\mathcal{O}(u^{-1})\right), \\
\mathbf{P}_4(u) &= A_4 \left(-e^{-\frac{1}{2T_H}}\right)^{+iu} \left(u+\mathcal{O}(u^{0})\right),
\end{aligned} \tag{116}$$

where $A_1 A_4 = A_2 A_3 = \frac{i}{\tanh^2\left(\frac{1}{4T_H}\right)}$ [1]. The exponential factor emerges from the twisted boundary conditions where they determined the twist variables as $\frac{1}{x_1} = \frac{1}{x_2} = x_3 = x_4 = -e^{-\frac{1}{2T_H}}$ and $y_1 = y_2 = \frac{1}{y_3} = \frac{1}{y_4} = 1$ [55]. The other Q-functions are

$$\begin{aligned}
\mathbf{Q}_1(u) &= B_1(1+\mathcal{O}(u^{-1})), \\
\mathbf{Q}_2(u) &= B_2(1+\mathcal{O}(u^{0})), \\
\mathbf{Q}_3(u) &= B_3(1+\mathcal{O}(u^{1})), \\
\mathbf{Q}_4(u) &= B_4(1+\mathcal{O}(u^{2})),
\end{aligned} \tag{117}$$

where

$$3B_1 B_4 = B_2 B_3 = -8i \cosh^4\left(\frac{1}{4T_H}\right), \tag{118}$$

$$A_1 = iA_2 = -A_3 = -iA_4 = \left(\tanh\frac{1}{4T_H}\right)^{-1}, \quad B_1 = B_2 = 1. \tag{119}$$

Equation (119) is a gauge choice due to some remnant symmetry (see the symmetries in section 2.3.2). In this gauge the components of $\mathbf{P}_a$ can transform into each other at leading order of their expansion

$$\mathbf{P}_1(u) \sim -\mathbf{P}_3(-u), \qquad \mathbf{P}_2(u) \sim \mathbf{P}_4(-u). \tag{120}$$

Branch cuts

The coupling dependency enters the Hagedorn QSC through branch cuts of the Q-functions. The exact structure was found in [1, 55] by constructing the T-system. $\mathbf{P}_a$ and $\mathbf{Q}_i$ are no longer polynomials but have Zhukowsky branch cuts

$$x(u) = \frac{u}{2g}\left(1+\sqrt{1-\frac{4g^2}{u^2}}\right) \tag{121}$$

in $u \in (-2g, 2g)$, where $g = \frac{\sqrt{\lambda}}{4\pi}$ depends on the 't Hooft coupling λ and is called the effective planar loop coupling. The analytic continuation of the Zhukowsky cut is

$\tilde{x}(u) = \frac{1}{x(u)}$ [73]. The branch cuts of the Hagedorn QSC have to be the opposite to the ones of the QSC due to the double Wick rotation. The simplest structure the Hagedorn QSC can take on is when one chooses the Riemann sheets such that $\mathbf{Q}_i$ has a single branch cut at $(-2g, 2g)$ and $\mathbf{P}_a$ has a long cut $(-\infty, -2g) \cup (2g, \infty)$ (see figs. 4 and 5) [1, 55, 73]. However, the long cut is inconvenient since $\mathbf{P}_a$ and $\mathbf{Q}_i$ have to satisfy the QQ-relations and should thus have similar properties. Instead of the long cut one can also choose the short cut of $\mathbf{P}_a$. But due to the QQ-relations it has an infinite set of cuts [73]. That emerges from the recursive formula eq. (101) by inserting it into the relation

$$\mathbf{P}_a = -Q^+_{a|i}\mathbf{Q}^i, \tag{122}$$

where we get

$$Q^-_{a|i} = Q^+_{a|i} + \mathbf{Q}_i\mathbf{Q}^j Q^+_{a|j}. \tag{123}$$

Combining those two functions

$$\begin{aligned}\mathbf{P}_a &= -\mathbf{Q}^i Q^+_{a|i} \\ &= -\mathbf{Q}^i \left(\delta^j_i + \mathbf{Q}^{[+2]}_i \mathbf{Q}^{j\,[+2]}\right) Q^{[+3]}_{a|j} \\ &= -\mathbf{Q}^i \left(\delta^j_i + \mathbf{Q}^{[+2]}_i \mathbf{Q}^{j\,[+2]}\right) \left(\delta^k_j + \mathbf{Q}^{[+4]}_j \mathbf{Q}^{k\,[+4]}\right) Q^{[+5]}_{a|k} = \cdots\end{aligned} \tag{124}$$

it is apparent that due to its recursive nature, $\mathbf{P}_a$ has an infinite set of short cuts. Those are located in the lower half plane at $(-2g - in, 2g - in)$ where $n \in \mathbb{N}_0$ (see fig. 6). The function $\mathbf{P}_a$ on the short cut is connected to the function on the long cut as an analytic continuation. The path in the upper half plane, i.e. above the branch point, we get a function $\mathbf{P}_a$ that is regular in the upper half plane (UHP) and has short cuts $(-2g - in, 2g - in)$ where $n \in \mathbb{N}_0$. Whereas, when taking the path in the lower half plane (LHP) we obtain a function $\tilde{\mathbf{P}}_a$ that is regular in the LHP but has the short cuts $(-2g + in, 2g + in)$ where $n \in \mathbb{N}_0$ (see fig. 7). $\tilde{\mathbf{P}}_a$ is the analytic continuation of $\mathbf{P}_a$ and it is found by replacing $x(u) \mapsto \tilde{x}(u) = \frac{1}{x(u)}$. For $\mathbf{Q}_i(u)$ it one can also find an analytic continuation $\tilde{\mathbf{Q}}_i(u)$ by replacing $x(u)$ with $\tilde{x}(u)$ [73].

Gluing condition

The Hagedorn QSC discussed so far has a significant problem. By construction, $\mathbf{P}_a$ satisfies all the QQ-relations and is well defined in the UHP. However, for $\tilde{\mathbf{P}}_a$ no such requirement exist. The analytic continuation in the Hagedorn QSC is solved using the complex conjugation. Thus, it is possible that the symmetry under complex conjugation

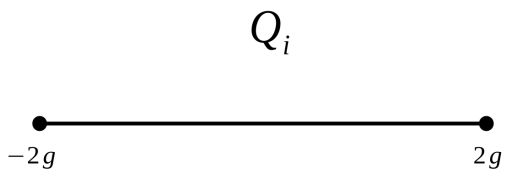

Figure 4: The figure shows the short branch cut for $\mathbf{Q}_i(u)$ in the interval $u \in (-2g, 2g)$.

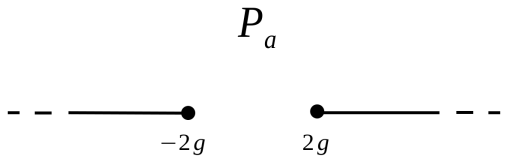

Figure 5: The figure shows the long branch cut for $\mathbf{P}_a(u)$ in the interval $u \in (-\infty, -2g) \cup (2g, \infty)$.

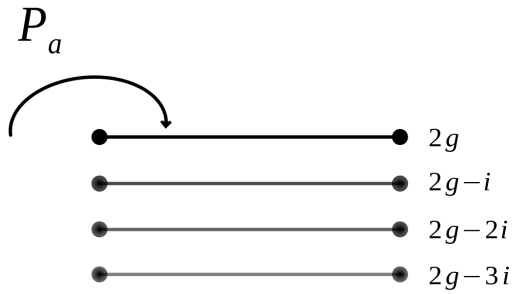

Figure 6: The figure shows the analytic continuation of $\mathbf{P}_a(u)$ in the upper half plane of the imaginary axis.

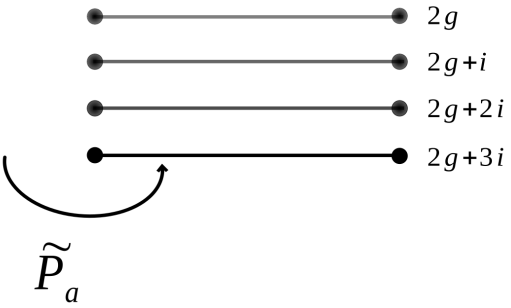

Figure 7: The figure shows the analytic continuation of $\tilde{\mathbf{P}}_a(u)$ in the lower half plane of the imaginary axis.

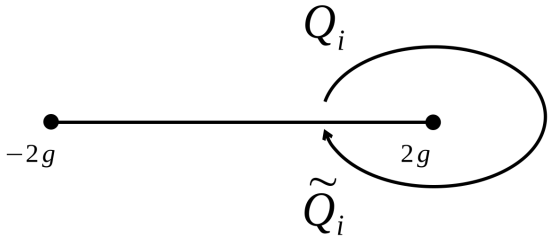

Figure 8: The figure shows the analytic continuation of $\tilde{\mathbf{Q}}(u)$.

is not satisfied. To re-establish that symmetry one can impose a set of equations that we will call gluing conditions [1, 73]

$$\tilde{\mathbf{P}}_a(u) = (-1)^{1+a}\overline{\mathbf{P}}_a(u) = (-1)^{1+a}\mathbf{P}_a(-u). \tag{125}$$

Those requirements close the QQ-relation equation system.

One additional property specific for the considered Hagedorn QSC is left-right symmetry. It is a symmetry that connects the $\mathfrak{su}(2|2)$ subalgebras of $\mathfrak{psu}(2,2|4)$. As a result we find relation between $\mathbf{P}_a$ and $\mathbf{P}^a$ in addition to Hodge-duality [1, 67]

$$\mathbf{P}_a = \chi_{ab}\mathbf{P}^b, \quad \mathbf{Q}_i = \chi_{ij}\mathbf{Q}^j, \tag{126}$$

where

$$\chi = \begin{pmatrix} 0 & 0 & 0 & 1 \\ 0 & 0 & -1 & 0 \\ 0 & 1 & 0 & 0 \\ -1 & 0 & 0 & 0 \end{pmatrix}. \tag{127}$$

That symmetry occurs in the Hagedorn QSC only if all the chemical potentials are set to zero [1].

2.3.4 Solution of Hagedorn QSC

The Hagedorn QSC problem can only be solved numerically for the Hagedorn temperature. The numeric method was proposed by Harmark and Wilhelm in [1] which is a modified version of an algorithm that was introduced in [76] to solve the QSC problem. The QQ-relations that are relevant for the following are

$$Q^+_{a|i} - Q^-_{a|i} = \mathbf{P}_a\mathbf{Q}_i, \tag{128}$$

$$\mathbf{P}_a = -\mathbf{Q}^i Q^+_{a|i}, \tag{129}$$

$$\mathbf{P}^a = \chi^{ab}\mathbf{P}_b, \quad \mathbf{Q}^i = \chi^{ij}\mathbf{Q}_j, \quad Q^{a|i} = \chi^{ab}\chi^{ij}Q_{b|j}. \tag{130}$$

We established the structure of $\mathbf{Q}_i(u)$ when discussing the analytic properties. The function has only one short branch cut at $(-2g, 2g)$ and we also now the asymptotic behaviour in eq. (117). Thus, with this information we are able to make a proper ansatz with B_i defined in eqs. (118) and (119)

$$\mathbf{Q}_i(u) = B_i(gx(u))^{i-1}\left(1 + \sum_{n=1}^{\infty}\frac{c_{i,n}(g)}{(gx(u))^{2n}}\right). \tag{131}$$

The coefficient $c_{3,1}$ is set to zero as a gauge choice. In the numeric implementation the sum is truncated to a maximal value $n \leq N$. One can then make an ansatz for the auxiliary function $Q_{a|i}$

$$Q_{a|i}(u) = \left(-e^{-\frac{1}{2T_H}}\right)^{-s_a i u} u^{p_{a|i}} \sum_{m=0}^{M} \frac{B_{a|i,m}}{u^m}. \tag{132}$$

For $a = 1, 2$ we use $s_a = 1$ and $p_{a|i} = a + u - 2$ whereas for the case $a = 3, 4$ we use $s_a = -1$ and $p_{a|i} = a + i - 4$. It is important to note, that eq. (132) is only converging when the real part of $is_a u$ is large, which means, for large imaginary u. Furthermore, in the following we using large u in the positive imaginary plane. Therefore, it is only possible to obtain convergent solutions when $a = 1, 2$ where in contrast the solutions for $a = 3, 4$ are exponentially divergent.
All the coefficients $c_{i,n}$ and $B_{a|i,n}$ together with the Hagedorn temperature T_H are unknown to this point. It is in our interest to reduce the number of unknowns. One way to perform this task is the comparison of the asymptotic functions in their leading behaviour. Inserting those into eq. (128), it is possible to express $B_{a|i,0}$ in terms of

$$B_{a|i,0} = -is_a \frac{e^{-\frac{1}{4T_H}}}{1 + e^{-\frac{1}{2T_H}}} A_a B_i. \tag{133}$$

For higher n one has to make use of a different approach. In order to do so, take eq. (128) and insert eq. (129) so that the function is free of $\mathbf{P}_a(u)$ and we find

$$Q^-_{a|i} = Q^+_{a|i} + \mathbf{Q}_i \mathbf{Q}^j Q^+_{a|j}. \tag{134}$$

To be able to solve this equation one might make an expansion in power of $\frac{1}{u}$ for large u of this expression

$$\left(-e^{-\frac{1}{2T_H}}\right)^{is_a u} u^{-p_{a|i}} \left(Q^+_{a|i} - Q^-_{a|i} + Q^+_{a|j} \mathbf{Q}^j \mathbf{Q}_k\right) = \sum_{l=1}^{\infty} u^{3-l} V_{a|i,l}. \tag{135}$$

Setting $V_{a|i,l}$ to zero yields the equations to determine $B_{a|i,n}$. Apart of that, also $c_{4,1}$ and $c_{4,2}$ are also determined that way. The equations can be solved numerically and deliver the approximate values for $B_{a|i,n}$ in dependence of the remaining $c_{i,n}$, T_H and g. To gain the approximate solution of $Q_{a|i}$ for the given sum $m \leq M$, one needs to find solutions for $V_{a|i,l} = 0$ where $l \leq m + 8$ [1].

With that $Q_{a|i}$ has been determined in the large u limit. With that we can now turn to finding $\mathbf{P}_a(u)$ using eq. (129). In order to acquire the function $Q_{a|i}$ for finite u, one can apply eq. (134) successively until one reaches $Q_{a|i}(u + i/2)$ for a set of points in

the interval $u \in (-2g, 2g)$. Hence, $\mathbf{P}_a(u)$ on the cut is then constructed by the truncated function $\mathbf{Q}_i$ in eq. (131) and the shifted function $Q^+_{a|i}$. Furthermore, taking the analytic continuation of the Zhukowsky variable $\tilde{x}(u) = \frac{1}{x(u)}$, we find the analytic continuation $\tilde{\mathbf{Q}}_i$ and thus

$$\tilde{\mathbf{P}}_a = -\tilde{\mathbf{Q}}^i Q_{a|i}. \tag{136}$$

Up until now, we have determined all the Q-functions in terms of T_H, g and the coefficients $c_{i,n}$, apart from $c_{4,1}$ and $c_{4,2}$. While keeping g as a free parameter, the other variables can be acquired by imposing the gluing conditions. This is done in form of a minimization function

$$F(T_H, \{c_{i,n}\}) = \sum_{a=1}^{2} \sum_{j=1}^{P} \left| \frac{\overline{\mathbf{P}_a(p_i)}}{\tilde{\mathbf{P}}_a(p_i)} + (-1)^a \right|^2. \tag{137}$$

Here p_i are P points living on the cut $p_i \in (-2g, 2g)$. Further, notice that the gluing conditions are only imposed for $a = 1, 2$ since those are the only solutions that converge. Equation (137) can then be solved by a Levenberg-Marquardt algorithm.

2.3.5 Hagedorn behaviour at any coupling

Considering the partition function for $\mathcal{N} = 4$ SYM on $\mathbb{R} \times S^3$

$$Z(T) = \mathrm{Tr}_{\mathbb{R}\times S^3}\, e^{-H/T} \tag{138}$$

which is just the general quantum mechanical formulation. Via the state-operator map explained in section 2.1.2 the partition function can be expressed on $\mathbb{R}^{1,3}$ instead of a sphere S^3

$$Z(T) = \mathrm{Tr}_{\mathbb{R}^{1,3}}\, e^{-D/T}, \tag{139}$$

where the dilatation operator is $D = D_0 + \delta D$ where δD is the anomalous part. The operators participating in the partition function are multi-trace and single-trace operators. In the planar limit the problem simplifies since the scaling dimension $\Delta = \Delta_0 + \delta\Delta$ of multi-trace operators reduces to the sum of the scaling dimension of the single-trace operators $\Delta_{MT} = \Delta_{ST} + \Delta_{ST} + \cdots$. So we only need the expression of the single-trace partition function which is

$$\begin{aligned} Z(T) &= \mathrm{Tr}_{\text{single-trace}} \left(e^{-\frac{1}{T}(D_0+\delta D)} \right) = \sum_{m=2}^{\infty} e^{-\frac{m}{2T}} Z_{\text{spin chain}, D_0=\frac{m}{2}}(T) \\ &= \sum_{m=2}^{\infty} e^{-\frac{m}{2T}} \left(\mathrm{Tr}_{\text{spin chain}, D_0=\frac{m}{2}}\, e^{-\frac{\delta D}{T}} \right). \end{aligned} \tag{140}$$

Defining the free energy of the spin chain as

$$F_m(T) = -T\frac{2}{m}\log\left(\mathrm{tr}_{spin-chain,\Delta_0=\frac{m}{2}}\left(e^{-\frac{\delta\Delta}{T}}\right)\right) \tag{141}$$

per units of the scaling dimension $D_0 = \frac{m}{2}$, the single-trace partition function is then

$$Z_{ST}(T) = \sum_{m=2}^{\infty} e^{\frac{m}{2T}(1+F_m(T))}. \tag{142}$$

By also counting all multi-trace operators, the entire partition function reads as

$$Z(T) = \exp\left(\sum_{n=1}^{\infty}\frac{1}{n}\sum_{m=2}^{\infty}(-1)^{m(n+1)}e^{\frac{m}{2T}(n+F_m(\frac{T}{n}))}\right). \tag{143}$$

The Hagedorn temperature is defined as the lowest temperature that gives rise to a singularity in the partition function. For $Z(T)$ in eq. (143) this is the case for $n = 1$. Hence, one has to find a singularity for

$$\sum_{m=2}^{\infty} e^{-\frac{m}{2T}(1+F_m(T)} \tag{144}$$

which is possible using the Cauchy root test. It states that a series $\sum_{n=1}^{\infty} a_n$ diverges if $r = \lim_{n\to\infty}\sqrt[n]{a_n} > 1$ and converges if $r < 1$. For eq. (144) the condition for divergence is

$$r = e^{-\frac{1}{2T}(1+F(T))} = 1 \tag{145}$$

where

$$F(T) = \lim_{m\to\infty} F_m(T) = -\lim_{m\to\infty}\frac{2T}{m}\ln Z_{\text{spin chain},D_0=\frac{m}{2}}(T). \tag{146}$$

The limit takes the classic scaling dimension which is exactly the limit we need to obtain the direct theory (see section 2.3.3). Thus, the condition for the free energy at the Hagedorn temperature is

$$F(T_H) = -1. \tag{147}$$

The free energy of the spin chain $F(T_H)$ was determined by Harmark and Wilhelm in [55].

Based on the numeric implementation described in section 2.3.4 it is possible to find the Hagedorn temperature for a large range of values for the coupling constant g. In [1] the Hagedorn temperature T_H has been evaluated as a function of g in the interval $[0, 3.24]$ which is depicted in fig. 9. In the figure one can see that the Hagedorn

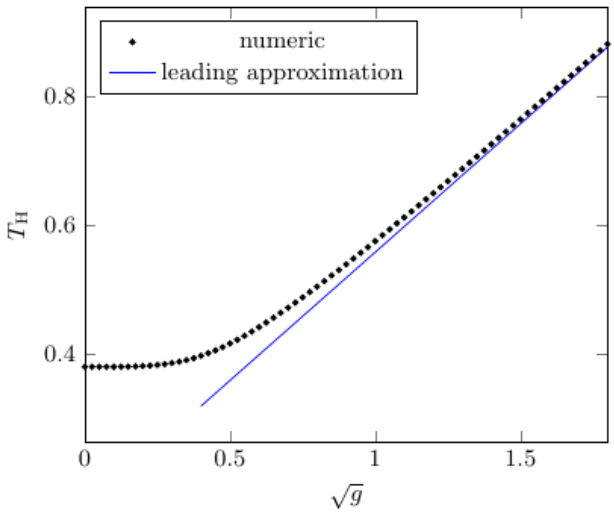

Figure 9: The plot shows the numeric solutions of the Hagedorn temperature T_H and the leading approximation function (defined in eq. (148)) as a function $\sqrt{g}$. The figure is taken from [1].

temperature has an asymptotically linear growth in the strongly coupled region. Therefore, the behaviour has been approximated using a linear function with correction terms up to order $\left(\frac{1}{\sqrt{g}}\right)^6$. Based on the found values it as been shown that the temperature approaches the value

$$T_H(g) \approx (0.399\ldots)\sqrt{g} \simeq \sqrt{\frac{g}{2\pi}} \tag{148}$$

for large 't Hooft coupling. Since we set $R = 1$ in the beginning the temperature is measured in units of R. The found result eq. (148) can be translated to the string theory side by using the relation for the radius of the sphere S^3 that we are working with $R = (4\pi\lambda)^{\frac{1}{4}} l_s$ (see section 2.2.1). In terms of string theory eq. (148) then is

$$T_H(g) \simeq \frac{1}{\sqrt{8}\pi l_s}. \tag{149}$$

This result is exactly the Hagedorn temperature for type IIB string theory on 10-dimensional Minkowski space [77].

3 Results

In the last section we saw that the Hagedorn QSC provides for a numerical approach to gain insights to the deconfinement phase transition/Hawking-Page transition for any values of the 't Hooft coupling. The numeric analysis however is limited for strong coupling due to the computational capacities. In practise obtaining values $\sqrt{g} \geq 2$ is effectively uneconomical. Therefore, it is of great interest to find an analytical solution to the Hagedorn QSC in the strongly coupled limit. In order to find such a description, we will start by analysing the numeric solutions of the Q-functions and try to find an analytic expression in the limit $g = \frac{\sqrt{\lambda}}{4\pi} \to \infty$.
The foundation of this study is the algorithm described in section 2.3.4 which was implemented in *Mathematica* by Harmark and Wilhelm in [1]. First we find the numeric solutions for $\mathbf{Q}_i$ (eq. (131)) and $\mathbf{P}_a$ on the cut (eq. (129)). The range of the coupling constant is chosen to be $0.53 \leq g \leq 3.52$. However, going from weak to strong coupling is rather difficult since the precision is decreasing very fast. In order to get reasonable results one can increase the working precision and the number of subleading orders in eq. (131). We chose the working precision as 300 and $N = 38$ terms for the sum in eq. (131). The high number of summands increases the computational capacities and slows down the algorithm at such rate that it is difficult to obtain results or very high g.

Hence, by solving the Hagedorn QSC, one can find the coefficients $c_{i,n}(u)$ for $\mathbf{Q}_i(u)$ and the values of the function $\mathbf{P}_a(u)$. In the following sections we are going to analyse those functions and try to find an analytic expression to describe their behaviour at strong coupling. The fits are all performed in *Mathematica* with the function `NonLinearFit[]`. As a measure of the goodness of the fit we are going to use the mean squared error (MSE)

$$MSE = \frac{1}{n}\sum_{i=1}^{n}(x_i - \bar{x}_i)^2\,, \tag{150}$$

where x_i is the value found by the algorithm and $\bar{x}_i$ the value of the fit.

We are starting the analysis of the Hagedorn QSC with the function $\mathbf{Q}_i(u)$ which is defined in eq. (131). The coefficients $c_{i,n}$ are the output of the minimization function except $c4,1$ and $c_{4,2}$ as well as $c_{3,1}$, which is set to zero (see section 2.3.4). The first four coefficients $c_{i,n}$ for $\mathbf{Q}_1(u)$ are shown in fig. 10 as a function of $\sqrt{g}$. One can see that each of the coefficients behave different to the others. Thus, it is difficult to find

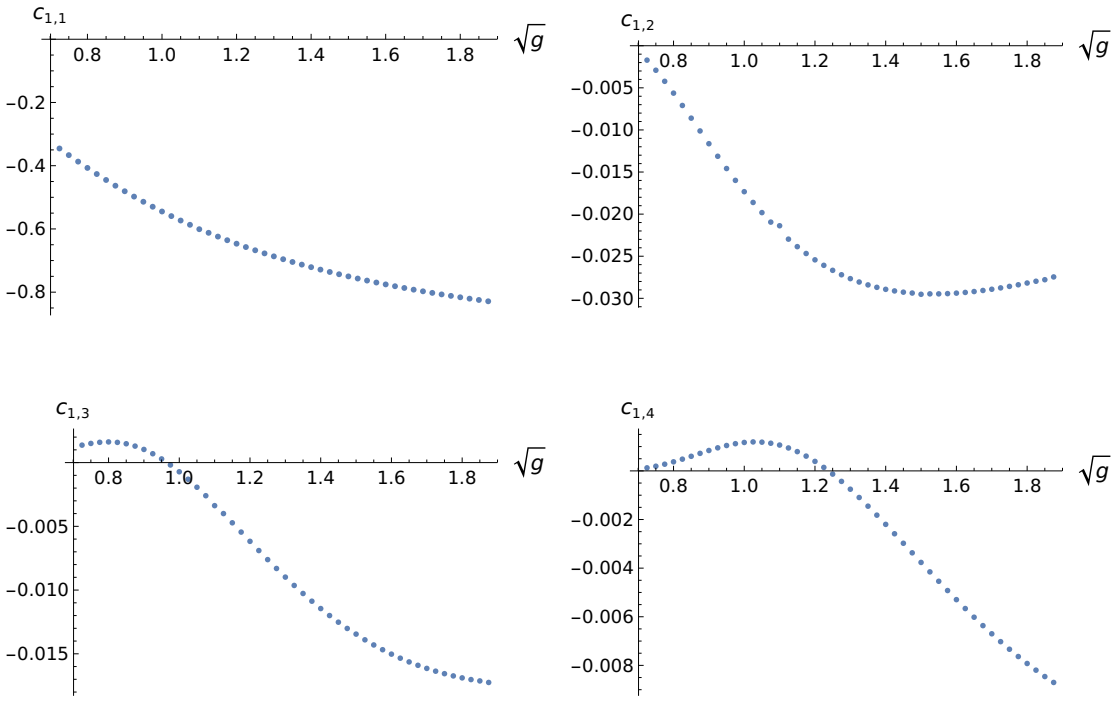

Figure 10: The first four coefficients of $\mathbf{Q}_1(u)$ eq. (131) plotted as a function of $\sqrt{g}$.

a function that would describe all the coefficients. One might also consider different dependencies of g, as $g^{\frac{1}{4}}$, g or g^2 (see appendix for plots). However, the behaviour of the coefficients is still not suitable for finding a common ansatz. Furthermore, in the considered range of g the functions do not converge for the limit $g \to \infty$. The same problems occur for $Q_i(u)$ for $i = 2, 3, 4$ (see appendix). Thus, it might be more effective to study the function $\mathbf{P}_a(u)$.

As already discussed in section 2.3.4, the function $Q_{a|i}(u)$ (eq. (132)) is exponentially small for $a = 1, 2$ and exponentially large for $a = 3, 4$. Since the function $\mathbf{P}_a(u)$ is constructed by eq. (129), it also has two convergent solutions and two divergent solutions. For $a = 1, 2$ the convergent solution is found by enforcing the asymptotic limit in the positive imaginary direction and further using eq. (134) to iteratively go down to the real axis by steps of i, as described in section 2.3.4. $P_{1,2}$ can be determined that way since they are the convergent solutions. However, in the case of $a = 3, 4$, $P_{3,4}$ are divergent. To find the finite solution for $a = 3, 4$ we can use the same procedure but in the negative imaginary limit. To do so, an equivalent to eq. (134) is needed to be found for which we can just use the relation eq. (128) and multiply it by $\mathbf{Q}_i$

$$\left(Q^{+}_{a|i} - Q^{-}_{a|i}\right) \mathbf{Q}^i = \mathbf{P}_a \mathbf{Q}_i \mathbf{Q}^i. \tag{151}$$

The RHS is equal to zero because of eq. (111). Equation (151) then reads as

$$Q^{+}_{a|i}\mathbf{Q}^{i} = Q^{-}_{a|i}\mathbf{Q}^{i} = -\mathbf{P}_{a} \tag{152}$$

and so the recursive relation eq. (128) reduces to

$$Q^{+}_{a|i} = \left(\delta^{j}_{i} - \mathbf{Q}_{i}\mathbf{Q}^{j}\right) Q^{-}_{a|j}. \tag{153}$$

That relation allows the asymptotic function to jump from the lower half plane to the real axis in steps of i. Hence, this procedure delivers the finite solutions $\mathbf{P}_3$ and $\mathbf{P}_4$.

The convergent solution of $\mathbf{P}_1(u)$ is exemplary shown in fig. 11 for all $\mathbf{P}_a(u)$. As one can see, the function has very high values and a steep slope. This is not convenient for a proper analysis. Hence, in the following we are going to construct a function that works as a good foundation for further analysis. The steepness of $\mathbf{P}_a$ indicates an underlying exponential function. This suspicion is consistent when considering the ansatz for $\mathbf{P}_a$ in the asymptotic limit (defined in eq. (116)) which includes an exponential prefactor. That factor can be rewritten as

$$\left(-e^{-\frac{1}{2T_H}}\right)^{\mp iu} = \left(-e^{-\frac{1}{2T_H}} + i0\right)^{\mp iu} = e^{\pm\pi u}\left(e^{-\frac{1}{2T_H}}\right)^{\mp iu}. \tag{154}$$

Thus, we obtain a product of a real exponential function and a phase. The real factor is the source of the steep slope and hence, by cancelling this factor it leaves us a good function for fitting

$$\widehat{\mathbf{P}}_{1,2}(u) = \mathbf{P}_{1,2}(u)e^{-\pi u} \tag{155}$$

$$\widehat{\mathbf{P}}_{3,4}(u) = \mathbf{P}_{3,4}(u)e^{+\pi u}. \tag{156}$$

Those function are depicted in figs. 12a to 12d. Since the function $\mathbf{P}_a(u)$ is ill-defined at the branch points $u = \pm 2g$ we would expect a series expansion for u.

One can see that the functions $\widehat{\mathbf{P}}_a$ are symmetric and anti-symmetric. To understand why they are behaving in that way we have to look at the gluing conditions eq. (125). Applying them to the asymptotic ansatz ensures that the functions $\mathbf{P}_1(u)$ and $\mathbf{P}_3(u)$ have only a real part whereas $\mathbf{P}_2(u)$ and $\mathbf{P}_4(u)$ are only imaginary. With those assumptions one can make an even more restricted ansatz for $\mathbf{P}_a(u)$ on the real

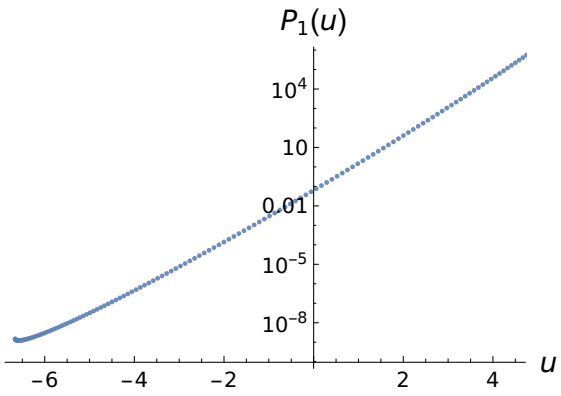

Figure 11: The figure shows the function $\mathbf{P}_1(u)$ in the interval $u \in (-2g, 2g)$ where the coupling $g = 3.33$ and the Hagedorn temperature $T_H = 0.8915$.

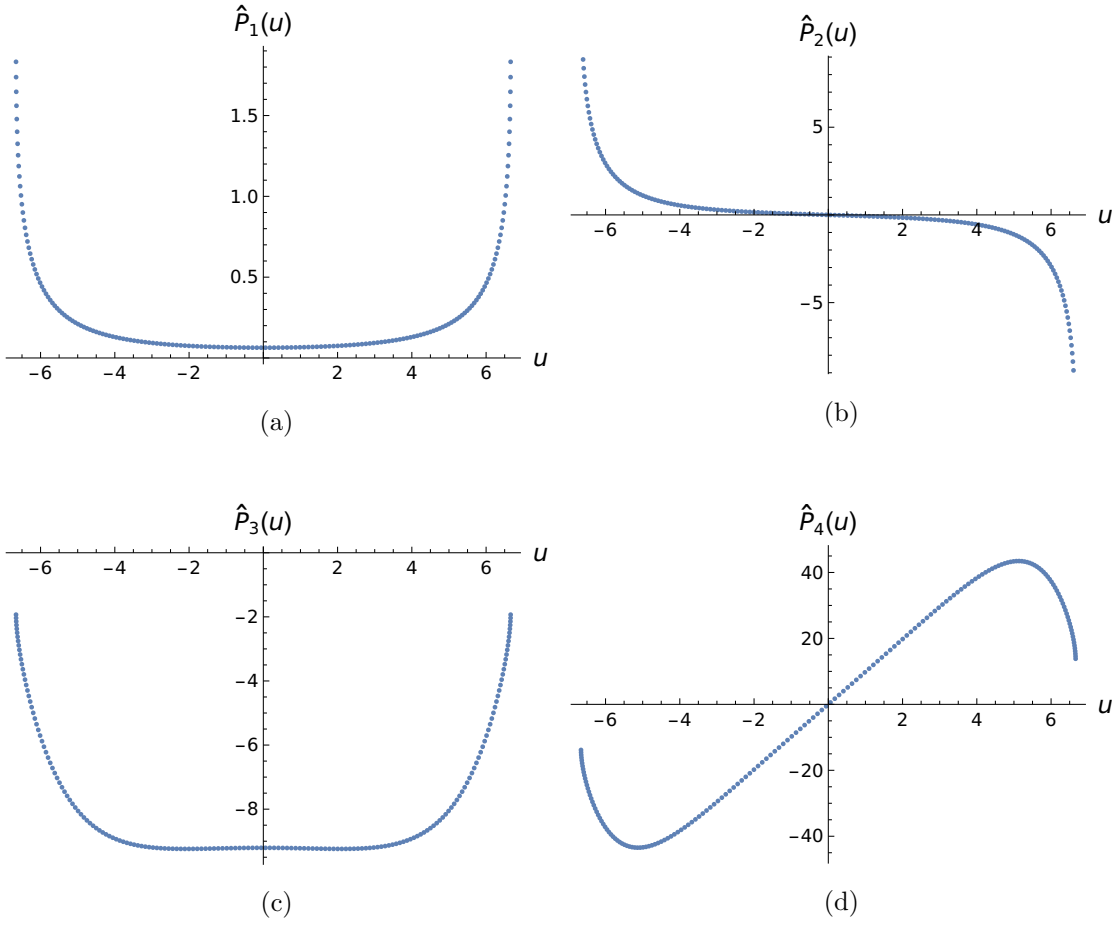

Figure 12: The figure shows $\widehat{\mathbf{P}}_a(u)$ in the interval $u \in (-2g, 2g)$ for a coupling constant $g = 3.33$ and $T_H = 0.8915$.

axis

$$\widehat{\mathbf{P}}_1(u) = \mathrm{Re}\left(\mathbf{P}_1 e^{-\pi u}\right) = \sum_{l=0}^{\infty} a_{1,l}(g) u^{2l}, \tag{157}$$

$$\widehat{\mathbf{P}}_2(u) = \mathrm{Im}\left(\mathbf{P}_2 e^{-\pi u}\right) = \sum_{l=0}^{\infty} a_{2,l}(g) u^{2l+1}, \tag{158}$$

$$\widehat{\mathbf{P}}_3(u) = \mathrm{Re}\left(\mathbf{P}_3 e^{+\pi u}\right) = \sum_{l=0}^{\infty} a_{3,l}(g) u^{2l}, \tag{159}$$

$$\widehat{\mathbf{P}}_4(u) = \mathrm{Im}\left(\mathbf{P}_4 e^{+\pi u}\right) = \sum_{l=0}^{\infty} a_{4,l}(g) u^{2l+1}, \tag{160}$$

where all the coefficients are functions of the planar coupling $g = \frac{\sqrt{\lambda}}{4\pi}$. Note, that the functions $\mathbf{P}_{2,4}(u)$ do not have any coefficient of zeroth order due to the gauge eq. (120) that requires $\mathbf{P}_{2,4}(u)$ to have a root at the point $u = 0$. The series ansatz in eqs. (157) to (160) has a convergence radius and hence, for a reasonable fit, only half of the points will be considered. For the fits we will only take $l = 8$. This order has been chosen considering the stability of the fit. The functions $\widehat{\mathbf{P}}_a(u)$ are depicted in figs. 13a to 13d for a certain value of $g = 3.33$ and $T_H = 0.8915$.

Furthermore, in order to calculate the analytic continuation one has to take $x(u) \to \frac{1}{x(u)}$ (see section 2.3.3). Figures 14a to 14d show the analytic continuations for $\tilde{\mathbf{P}}_a$. Comparing those functions, we can see that $\mathbf{P}_a$ and $\tilde{\mathbf{P}}_a$ are related as

$$\mathbf{P}_1(u) = -\tilde{\mathbf{P}}_3(u), \tag{161}$$

$$\mathbf{P}_2(u) = -\tilde{\mathbf{P}}_4(u), \tag{162}$$

$$\mathbf{P}_3(u) = -\tilde{\mathbf{P}}_1(u), \tag{163}$$

$$\mathbf{P}_4(u) = -\tilde{\mathbf{P}}_2(u). \tag{164}$$

These equalities stand directly in relation with the gauge choice eq. (120). One can see that by using the gluing conditions eq. (125) and transforming $\tilde{\mathbf{P}}_a(u)$ accordingly it is possible to obtain eq. (120). The gauge choice was initially made in the large u expansion for the leading order coefficients. However, it seems that it is valid on the cut as well.

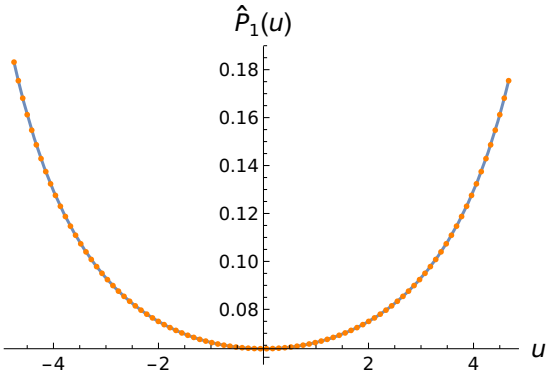

(a) $\widehat{\mathbf{P}}_1(u)$ with an $MSE = 9.24462 \times 10^{-17}$

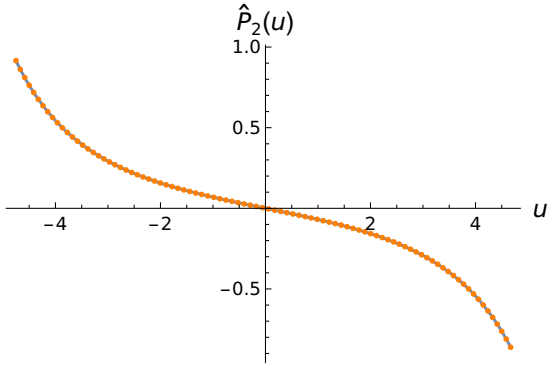

(b) $\widehat{\mathbf{P}}_2(u)$ with an $MSE = 8.05215 \times 10^{-16}$

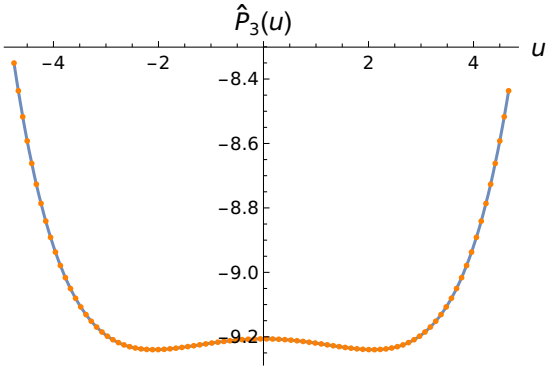

(c) $\widehat{\mathbf{P}}_3(u)$ with an $MSE = 1.44203 \times 10^{-18}$

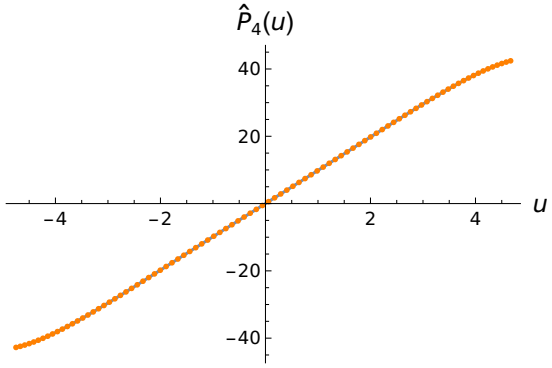

(d) $\widehat{\mathbf{P}}_4(u)$ with an $MSE = 8.03922 \times 10^{-18}$

Figure 13: The figure shows $\widehat{\mathbf{P}}_a(u)$ in the interval $u \in (-1.46g, 1.44g)$ for a coupling constant $g = 3.33$ and $T_H = 0.8915$. The orange dots are the numeric solutions from the algorithm while the blue line is the fit.

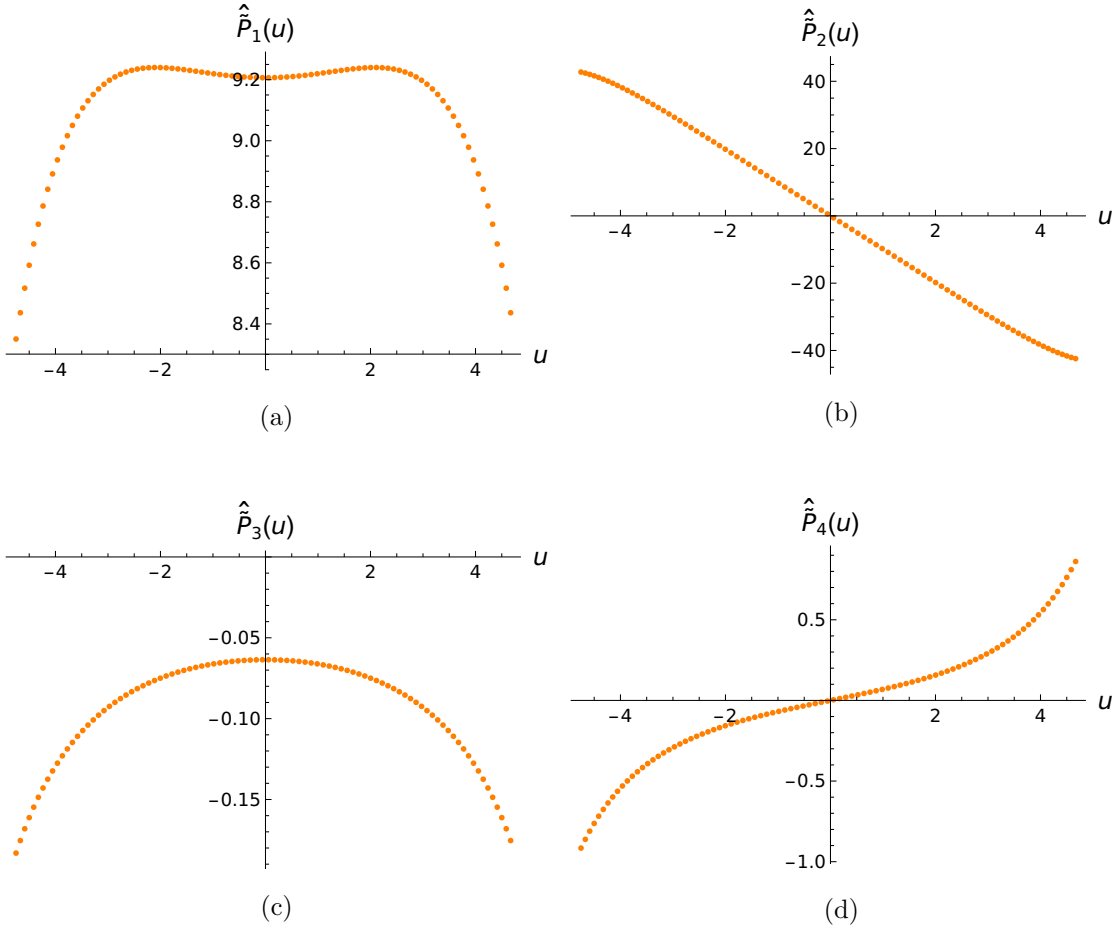

Figure 14: The figure shows $\hat{\tilde{\mathbf{P}}}_a(u)$ in the interval $u \in (-1.46g, 1.44g)$ for a coupling constant $g = 3.33$ and $T_H = 0.8915$.

The next step in understanding the function $\mathbf{P}_a(u)$ is to determine the analytic behaviour of the coefficients $a_{a,l}(g)$ eqs. (157) to (160) in the strong coupling limit. To do so, we can make a first ansatz for the case of $a = 1, 2$

$$\ln\left(a_{1,l}(g)\right) = b_0\sqrt{g} + b_1 + b_2\frac{1}{\sqrt{g}} + \cdots . \tag{165}$$

$$\ln\left(-a_{2,l}(g)\right) = b_0\sqrt{g} + b_1 + b_2\frac{1}{\sqrt{g}} + \cdots . \tag{166}$$

The coefficients seem like they would behave exponentially and we thus try to fit the logarithmic values for $a_{a,l}$. The first two coefficients for the case $g = 3.33$ and $T_H = 0.8915$ are shown in figs. 15a to 15d. As one can see, they approach a linear behaviour, especially when looking at higher values of $\sqrt{g}$. Further, the coefficients $a_{1,1}$ and $a_{2,1}$ are not converging well compared to the other two coefficients. This is due to the convergence radius of the ansatz eqs. (165) and (166) and thus it is valid to cut off data points in the lower $\sqrt{g}$ region. We chose to cut off the first 15 points which allow the fit to have a higher accuracy (see figs. 16a and 16b).

One might now also check whether the dependency of $\sqrt{g}$ is the correct. For that we compare the errors of the fits with different dependencies as they are listed in table 1. It displays the mean squared error eq. (150) for a linear fit and with an additional correction term of first order in $\frac{1}{\sqrt{g}}$, as in eqs. (165) and (166). The error for a $\sqrt{g}$ dependence is in fact the smallest and hence we deduce that this is the correct dependence.

The next point that needs to be discussed is the order of corrections. We fitted the coefficients using functions with corrections up to seventh order of $\frac{1}{\sqrt{g}}$. The main interest lies in the behaviour of the leading term b_0 since the objective is to take $g \to \infty$ eventually. The values b_0 for each coefficient $a_{a,l}$ are depicted in fig. 17a. The plot for $a_{1,0}$ and $a_{2,0}$ figs. 17a and 17d show both a decreasing behaviour until $N = 4$, which means $\left(\frac{1}{\sqrt{g}}\right)^4$. After that point, b_0 starts to show oscillating behaviour. The number of data points is 33, thus, when fitting it with a polynomial of corrections up to order seven, it is a loss of nine degrees of freedom in the fit. If there are sufficient fitting variables, it is always possible to find a good fit for any function. Therefore, above a certain number of correction terms the fitted coefficients are not reliable anymore. As a criterion, we say that when the value of b_0 reaches its first maximum or minimum depending on N this value will be the most reliable one. So, for $a_{1,0}$ as well as for $a_{2,0}$ the coefficient b_0 can be estimated as $b_0 = -2,3\ldots$. The first digit seems like a trustworthy choice since it is valid in the cases $4 \leq N \leq 6$. The leading order coefficient in $a_{1,1}$ and $a_{2,1}$ (figs. 17c and 17d) is increasing until $N = 3$. For higher orders of correction the values start

oscillating similar to the case $a_{1,0}$ and $a_{2,0}$. However, it starts to do so already at lower orders N since they have less data points then $a_{1,0}$ and $a_{2,0}$. The best approximation for b_0 in this case is $b_0 = -2,8\ldots$.
We have only studied the coefficients $l = 0,1$ of eqs. (157) and (158) here, although one could use the same arguments for the coefficients of higher l. However, due to the convergence radius of the ansatz eqs. (165) and (166), we would need to cut off too many points for a proper analysis.

Following this example we can make another possible ansatz for $a_{1,l}$ and $a_{2,l}$. Instead of considering the logarithmic value we can use the original ones and make an exponential ansatz

$$a_{a,l}(g) = e^{-b\sqrt{g}}(b_1 + b_2\frac{1}{\sqrt{g}} + \cdots) \quad \text{for} \quad a = 1,2. \tag{167}$$

The fits are depicted in figs. 18a to 18d where we already cut off 15 data points from below for $a_{1,1}$ and $a_{2,1}$ due to the convergence radius as we did for the other ansatz. Furthermore, we can again check whether the dependence of the $\sqrt{g}$ is valid or not by comparing the errors. Here it is the same result as for the case above, the accuracy of the fit is the best for a $\sqrt{g}$ dependence. The next step is to find a good parameter in the exponential function b. Therefore, consider the plots in figs. 19a to 19d which show the b by increasing the order of the correction order N in $\frac{1}{\sqrt{g}}$. The reported values seem in general a bit more stable than the ones in figs. 17a to 17d for larger corrections. However, they seem to oscillate strongly already for lower orders of correction N. The observed different behaviour to the previous case may be explained in this way. The corrections are of polynomial form and are all multiplied by the same exponential factor. Therefore, they are not able to affect the exponential prefactor as much as for example for the purely polynomial ansatz in eqs. (165) and (166).

Table 1: List of the MSE of $a_{1,0}$ and $a_{2,0}$ defined in eqs. (165) and (166) with different dependencies on g for an exponential fit and one with an additional first order correction term

$\ln(a_{1,0})$		
	linear	correction
g	5.53×10^{-3}	3.77×10^{-4}
$g^{\frac{1}{2}}$	6.82×10^{-5}	1.18×10^{-6}
$g^{\frac{1}{4}}$	2.68×10^{-3}	4.11×10^{-5}

$\ln(-a_{2,0})$		
	linear	correction
g	9.24×10^{-3}	1.34×10^{-4}
$g^{\frac{1}{2}}$	7.50×10^{-4}	2.21×10^{-6}
$g^{\frac{1}{4}}$	4.30×10^{-2}	2.47×10^{-3}

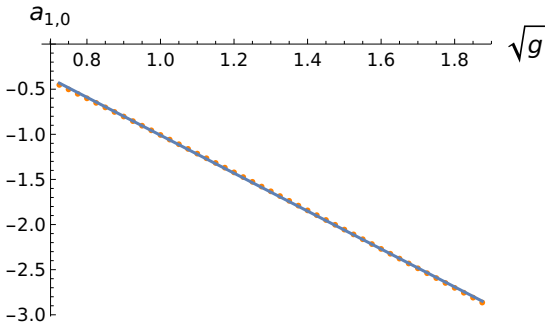

(a) $\ln(a_{1,0})(g) = 1.09095 - 2.10119\sqrt{g}$ with $MSE = 0.0000681955$

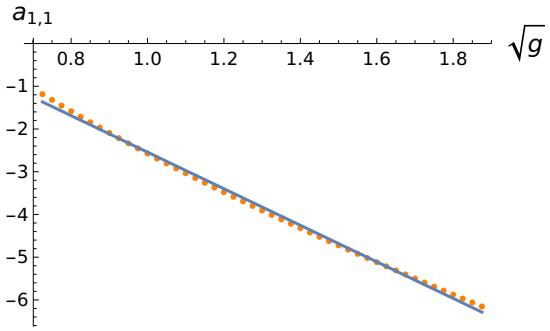

(b) $\ln(a_{1,1})(g) = 1.73449 - 4.27744\sqrt{g}$ with $MSE = 0.000100056$

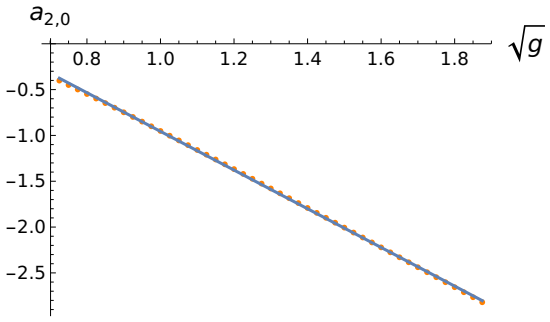

(c) $\ln(-a_{2,0})(g) = 1.15407 - 2.11028\sqrt{g}$ with $MSE = 0.00546094$

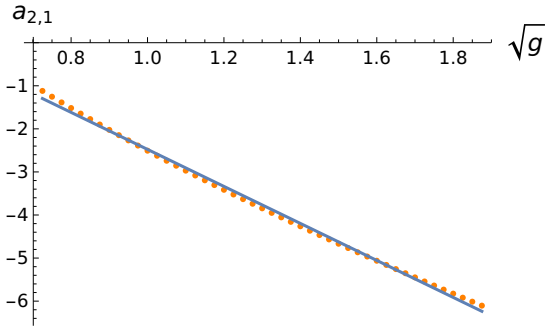

(d) $\ln(-a_{2,1})(g) = 1.81849 - 4.29564\sqrt{g}$ with $MSE = 0.00527707$

Figure 15: The figures show the dependency of the coefficients $a_{a,l}$ of $\sqrt{g}$ and a fitted linear function (blue line).

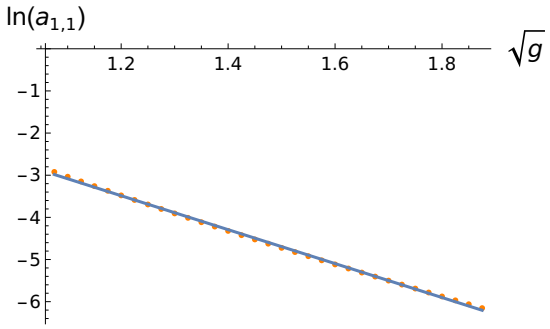

(a) $\ln(a_{1,1})(g) = 1.34426 - 4.02582\sqrt{g}$ with $MSE = 0.000749767$

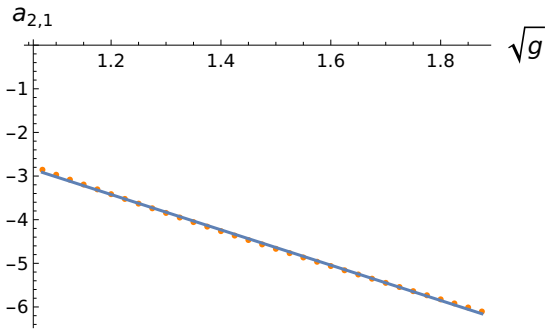

(b) $\ln(-a_{2,1})(g) = 1.43418 - 4.04787\sqrt{g}$ with $MSE = 0.000752288$

Figure 16: The figures show the dependency of the coefficients $a_{a,l}$ of $\sqrt{g}$ as in figs. 15b and 15d in the range $\sqrt{g} \in [1.075, 1, 875]$. The fitted function is indicated as blue line and the data as orange dots.

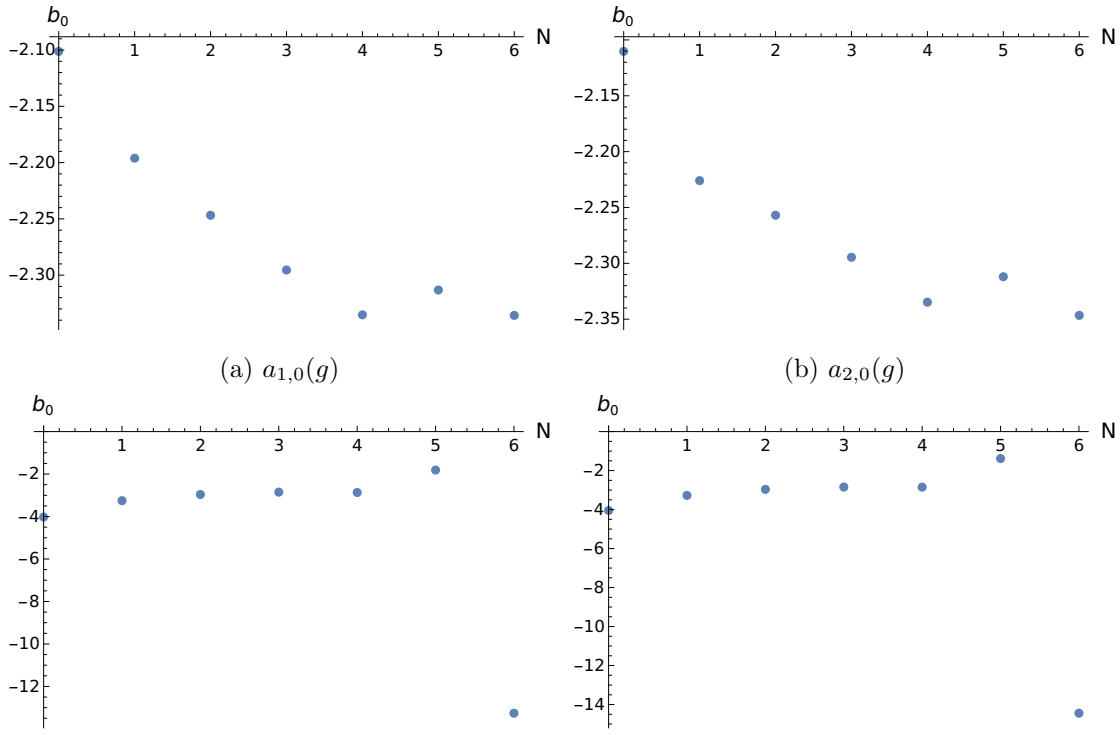

(a) $a_{1,0}(g)$

(b) $a_{2,0}(g)$

(c) $a_{1,1}(g)$

(d) $a_{2,1}(g)$

Figure 17: The figures show the leading order coefficient b_0 for $a_{a,l}$ defined in eqs. (165) and (166). The axis N indicates the number of the order of correction in $\frac{1}{\sqrt{g}}$. See table 4 in the appendix for the exact values.

If we turn to $a_{3,l}$ and $a_{4,l}$, we find that they behave completely different to $a_{1,l}$ and $a_{2,l}$. While the coefficients $a_{3,0}$ $a_{4,0}$ look like polynomials (see figs. 20a and 20b), the coefficients $a_{3,l}$ and $a_{4,l}$ for higher l have an exponential appearance. However, they are not entirely exponential since there exists a root. Therefore, the ansatz

$$a_{a,l} = e^{-bf(g)} \left(b_0 f(g) + b_1 + b_2 \frac{1}{f(g)} + \cdots \right) \quad \text{for} \quad a = 3, 4 \tag{168}$$

might be able to describe the function for $a = 3, 4$ as a function of $f(g)$ where $f(g)$ has yet to be determined. So, let us first consider $a_{3,0}$ and $a_{4,0}$ which are displayed in figs. 20a and 20b. Comparing the MSE of the fits for different functions of g (see table 3), it suggests that $a_{3,0}$ and $a_{4,0}$ are in fact depending on g and not $\sqrt{g}$. Going to the next order of l, we have to cut off the first 15 values again due to the convergence radius. The dependency of the coefficients is also listed in table 3. It is obvious that the coefficients $a_{3,1}$ and $a_{4,1}$ are best described by a $\sqrt{g}$ dependency. So, we found that for $l = 0$ in eq. (168) the function $f(g) = g$, whereas the coefficients for $l > 0$ are better described by $f(g) = \sqrt{g}$. One way to combine those dependencies is by using these function

$$a_{a,l} = e^{-b\sqrt{g}} \left(b_0 g + b_1 + b_2 \frac{1}{g} + \cdots \right) \quad \text{for} \quad a = 3, 4, \tag{169}$$

where the exponent depends on $\sqrt{g}$, while the linear term and the corrections depend on g. It is a compromise the fits are not as good as the other as one can see in figs. 22a to 22d. However, it would provide a description for all the coefficients. The stability of the exponential value are rather stable for $a_{3,0}$ and $a_{4,0}$, but not for $a_{3,1}$ and $a_{4,1}$. Therefore, it is not quite clear what the correct ansatz for $a = 3, 4$ is eq. (168). Therefore, it is not clear what the correct description is for $a = 3, 4$.

Table 2: List of the MSE of $a_{1,0}$ and $a_{2,0}$ defined in eq. (167) with different dependencies on g for an exponential fit and one with an additional first order correction term

$a_{1,0}$		
	exponential	correction
g	2.28×10^{-4}	8.25×10^{-6}
$g^{\frac{1}{2}}$	3.21×10^{-6}	4.81×10^{-8}
$g^{\frac{1}{4}}$	1.13×10^{-4}	8.68×10^{-6}

$a_{2,0}$		
	exponential	correction
g	2.36×10^{-4}	1.02×10^{-5}
$g^{\frac{1}{2}}$	6.21×10^{-6}	2.49×10^{-8}
$g^{\frac{1}{4}}$	1.40×10^{-4}	1.19×10^{-5}

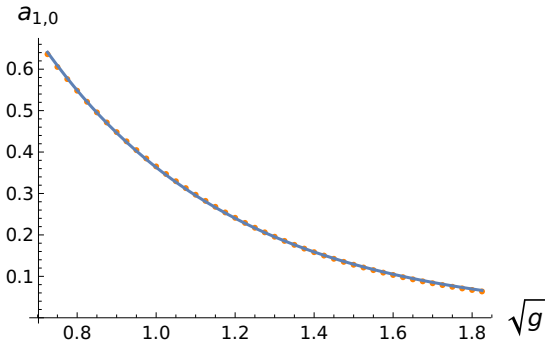

(a) $a_{1,0}(g) = 2.86709\ e^{-2.06641\sqrt{g}}$ with $MSE = 3.20934 \times 10^{-6}$

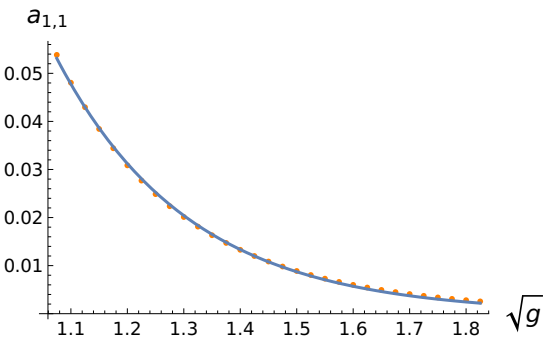

(b) $a_{1,1}(g) = 5.12843\ e^{-4.2512\sqrt{g}}s$ with $MSE = 9.37811 \times 10^{-8}$

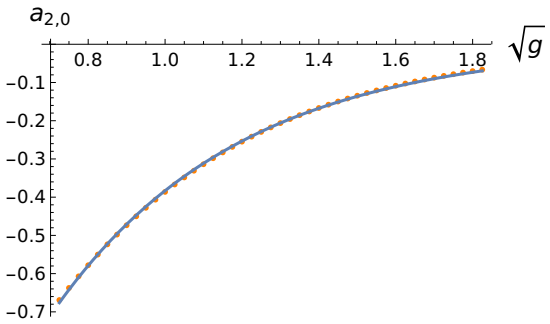

(c) $a_{2,0}(g) = -3.0257\ e^{-2.06684\sqrt{g}}$ with $MSE = 6.21246 \times 10^{-6}$

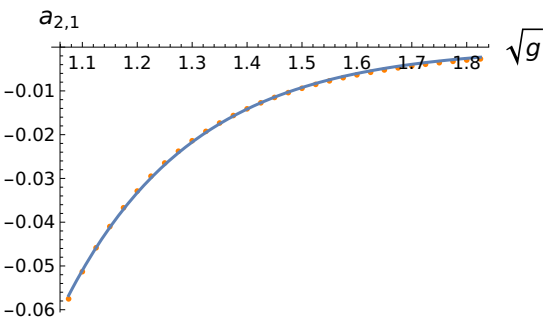

(d) $a_{2,1}(g) = -5.6158\ e^{-4.27398\sqrt{g}}$ with $MSE = 1.04241 \times 10^{-7}$

Figure 18: The figures show the dependency of the coefficients $a_{a,l}$ of $\sqrt{g}$ and a fitted exponential function (blue line).

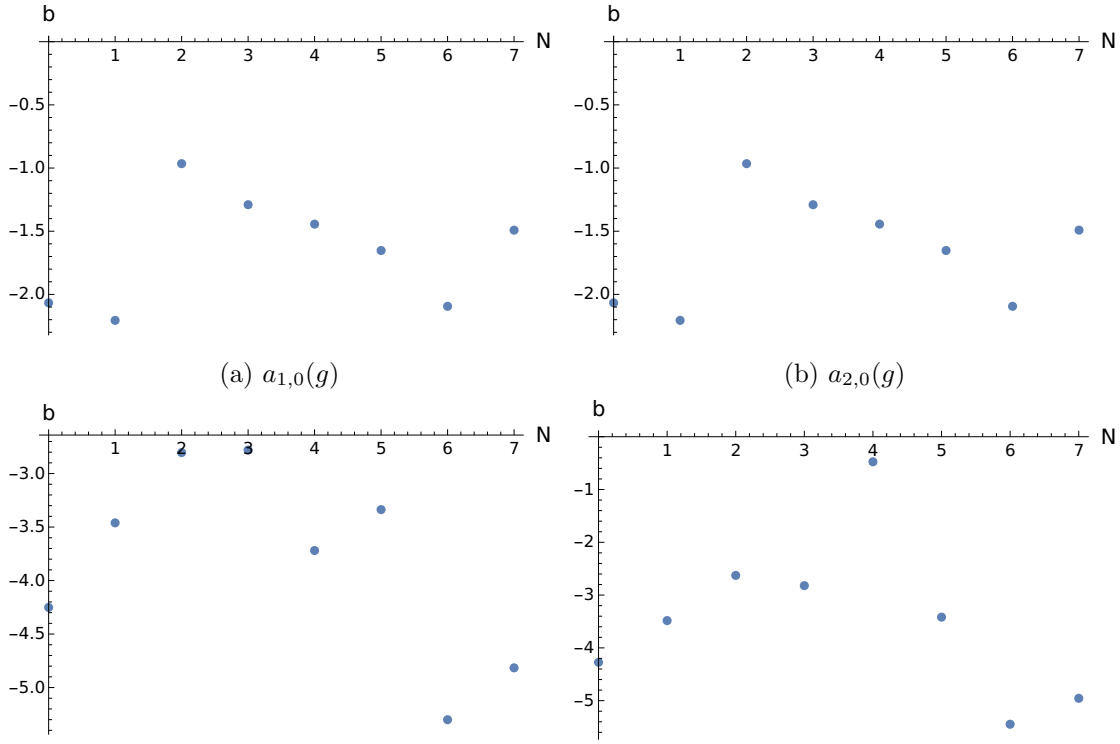

(a) $a_{1,0}(g)$ (b) $a_{2,0}(g)$

(c) $a_{1,1}(g)$ (d) $a_{2,1}(g)$

Figure 19: The figures show the leading order coefficient b for $a_{a,l}$ defined in eq. (167). The axis N indicates the number of the order of correction in $\frac{1}{\sqrt{g}}$. See table 5 in the appendix for the exact values.

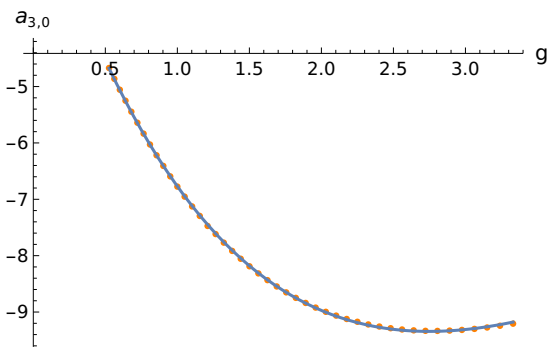

(a) $a_{3,0}(g) = e^{-0.345457g}(-1.22187 - 8.3409g)$ with $MSE = 1.03493 \times 10^{-4}$

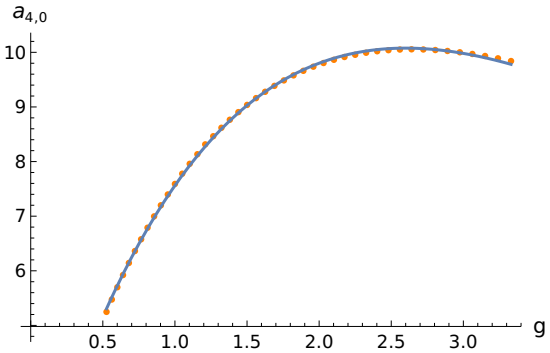

(b) $a_{4,0}(g) = e^{-0.362405g}(1.49403 + 9.3694g)$ with $MSE = 6.90273 \times 10^{-4}$

Figure 20: The figures show the dependency of the coefficients $a_{a,0}$ of g and a corresponding fitted function (blue line).

Table 3: List of the MSE of $a_{3,0}$ and $a_{4,0}$ with different dependencies on g for an exponential fit and one with a first order correction term

$a_{3,0}$		
	exponential	correction
g^2	8.58×10^{-2}	0.012
g	1.03×10^{-4}	6.37×10^{-5}
$g^{\frac{1}{2}}$	0.01	6.13×10^{-4}

$a_{4,0}$		
	exponential	correction
g^2	0.11	0.013
g	6.90×10^{-4}	9.40×10^{-5}
$g^{\frac{1}{2}}$	9.29×10^{-3}	6.24×10^{-4}

$a_{3,1}$		
	exponential	correction
g	1.14×10^{-5}	5.98×10^{-5}
$g^{\frac{1}{2}}$	6.58×10^{-7}	5.98×10^{-7}
$g^{\frac{1}{4}}$	3.69×10^{-6}	6.96×10^{-7}

$a_{4,1}$		
	exponential	correction
g	1.63×10^{-5}	5.97×10^{-7}
$g^{\frac{1}{2}}$	5.27×10^{-7}	5.26×10^{-7}
$g^{\frac{1}{4}}$	3.4×10^{-6}	5.58×10^{-7}

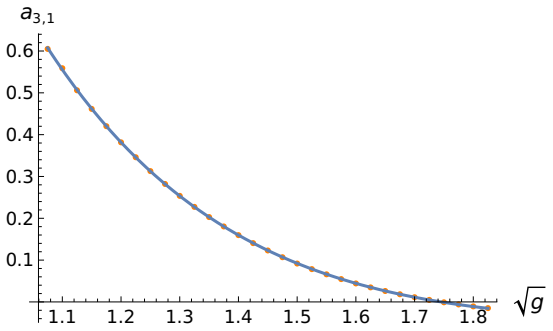

(a) $a_{3,1}(g) = e^{-2.06863\sqrt{g}}(14.6197 - 8.37681\sqrt{g})$ with $MSE = 6.57642 \times 10^{-7}$

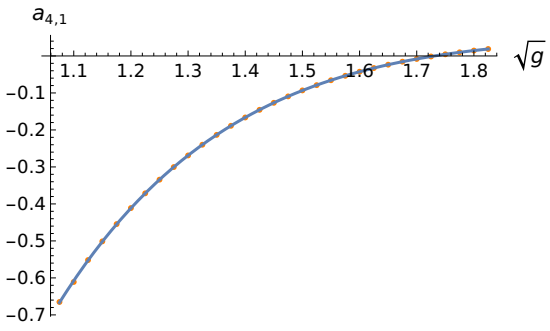

(b) $a_{4,1}(g) = e^{-2.16951\sqrt{g}}(-18.1237 + 10.4702\sqrt{g})$ with $MSE = 5.26568 \times 10^{-7}$

Figure 21: The figures show the dependency of the coefficients $a_{a,1}$ of $\sqrt{g}$ and a corresponding fitted function (blue line).

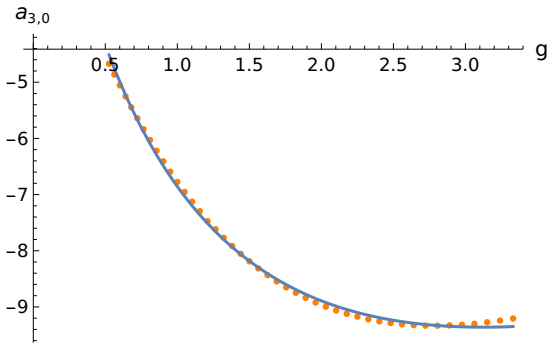

(a) $a_{3,0}(g) = e^{-1.16578g}(2.23222 - 24.235g)$ with $MSE = 4.43222 \times 10^{-3}$

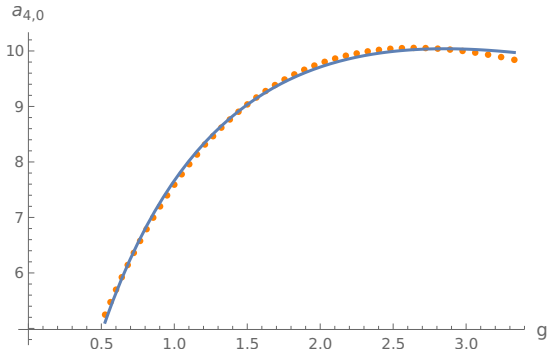

(b) $a_{4,0}(g) = e^{-1.22425g}(-2.70899 + 28.7777g)$ with $MSE = 3.54639 \times 10^{-3}$

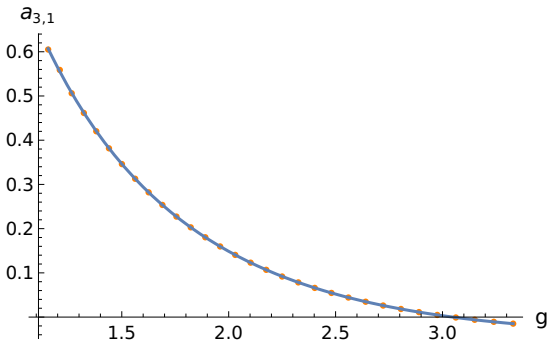

(c) $a_{3,1}(g) = e^{-2.40589\sqrt{g}}(12.9861 - 4.26071g)$ with $MSE = 6.01503 \times 10^{-7}$

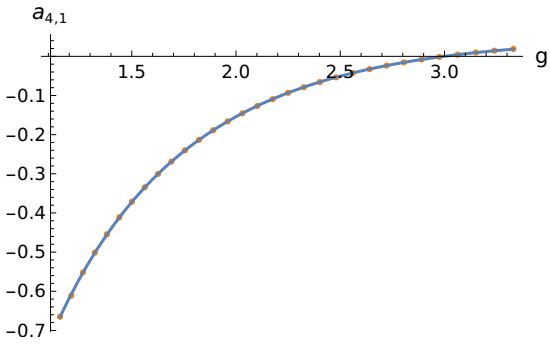

(d) $a_{4,1}(g) = e^{-2.50817\sqrt{g}}(-16.074 + 5.36206g)$ with $MSE = 5.79453 \times 10^{-7}$

Figure 22: The figures show the dependency of the coefficients $a_{a,l}$ of g, defined in eq. (169), and a corresponding fitted function (blue line).

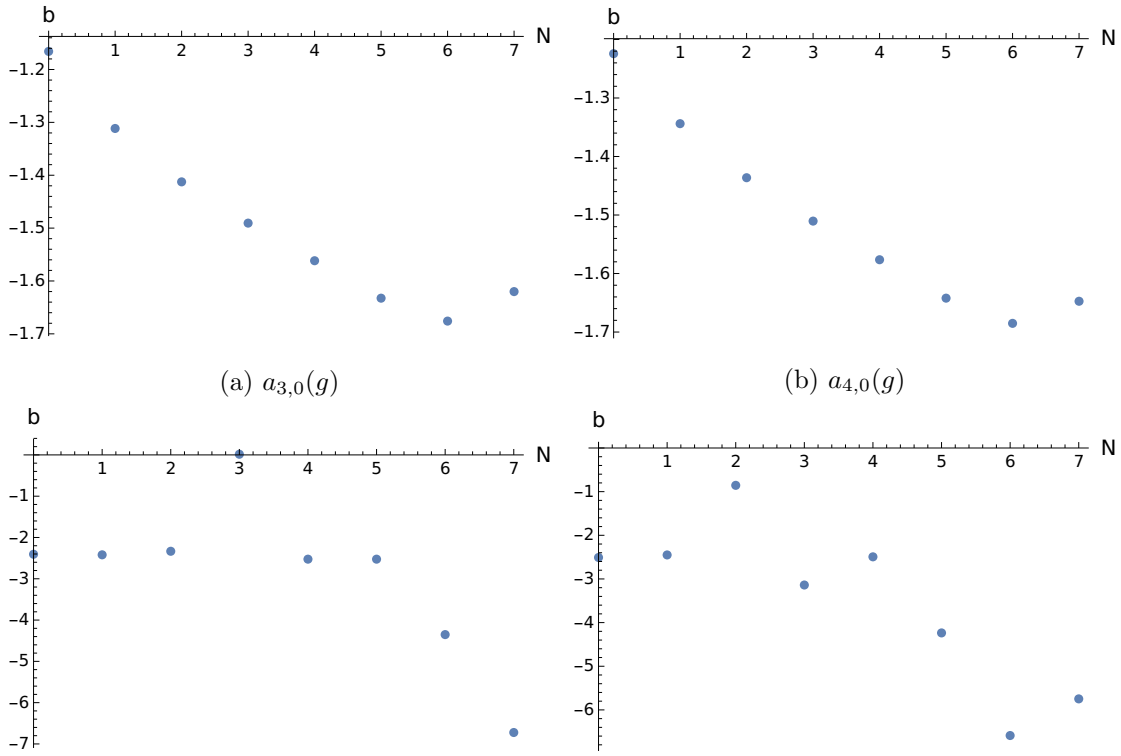

(a) $a_{3,0}(g)$ (b) $a_{4,0}(g)$

(c) $a_{3,1}(g)$ (d) $a_{4,1}(g)$

Figure 23: The figures show the leading order coefficient b for $a_{a,l}$ defined in eq. (169). The axis N indicates the number of the order of correction. The number N indicates the order of the correction in $\frac{1}{\sqrt{g}}$. See table 6 in the appendix for the exact values.

4 Discussion & Outlook

In this work we have analysed the behaviour of the Q-functions in the strong coupling limit. The foundation has been the numeric results obtained by the algorithm described in section 2.3.4. For $\mathbf{Q}_i(u)$ (see eq. (131)) we have not been able to find any conclusive ansatz for the coefficients $c_{i,n}$. The main problem was that the coefficients $c_{i,n}$ were not converging for $g \to \infty$, in the considered interval of g. Therefore, we have turned to the function $\mathbf{P}_a(u)$ instead, where we have been able to make an series expansion as an ansatz. Afterwards, we have studied the coefficients of this series expansion. We have used two different ansätze for $a = 1, 2$ to determine which one agrees the best. The first one is defined in eqs. (165) and (166) and we have found that the fit describes the function well. However, above a certain order of correction the values for the leading order start oscillating which makes it difficult to determine a trustworthy leading value. The second ansatz is defined in eq. (167). The mean squared error eq. (150) is here in general lower than for the first ansatz. Furthermore, the exponential dependency is rather stable does not start to have large oscillations for higher orders of correction compared to the first ansatz. Nonetheless, it is not obvious whether the discovered exponential dependence can be trusted since it is not stable when adding corrections. The results for $a = 3, 4$ are behaving in a completely different way to the ones for $a = 1, 2$. The main difficulty is that the coefficients of the series expansion of $\mathbf{P}_3$ and $\mathbf{P}_4$ have an polynomial dependence in addition to the exponential. This is unexpected since we have not found any obvious reason for this behaviour.

The analysis of the Q-function for strong coupling needs further investigation. The main limiting factor in this analysis was the lack of data for even higher coupling. Hence, for future studies the most important task might be to find more data points for even higher g. To achieve that, it would be advantageous to find a more effective algorithm so that it does not consume as much time and computing capacity to solve the Hagedorn QSC for even higher coupling g. Having more data for the fit, the problem with the stability of the leading order might be solved. Furthermore, it would be possible to study also higher order coefficients of $\mathbf{P}_a(u)$.
The analysis of $\mathbf{P}_3(u)$ and $\mathbf{P}_4(u)$ could also profit from more solutions for higher coupling. Besides, one way to find the reason for the behaviour of their coefficients is to look at the T-or Y-system again and try to find evidence for this behaviour. When this question has been answered, it also might be more clear which function describes $\mathbf{P}_1$ and $\mathbf{P}_2$ well.
When further analysis of $\mathbf{P}_a$ provides an ansatz for the strong coupling limit, it is pos-

sible to solve the Baxter-equation in eq. (103) to get a solution for $\mathbf{Q}_i(u)$ and thus, for the Hagedorn QSC. This might enable us to find a perturbative theory around it.

Acknowledgements

I would like to thank my supervisor Matthias Wilhelm for all the guidance and support during the process of this project and who always found the time to answer questions. Furthermore, I want to thank Troels Harmark and Matthias Wilhelm for providing their Mathematica code and all the numeric results which were the foundation for this work.
Additionally, I owe thanks to Edith Egler, Martina Hosner and Barbara Penzinger for proofreading the thesis. And lastly, I would like to thank Fynn Wolf and my family for all the moral support.

Appendix

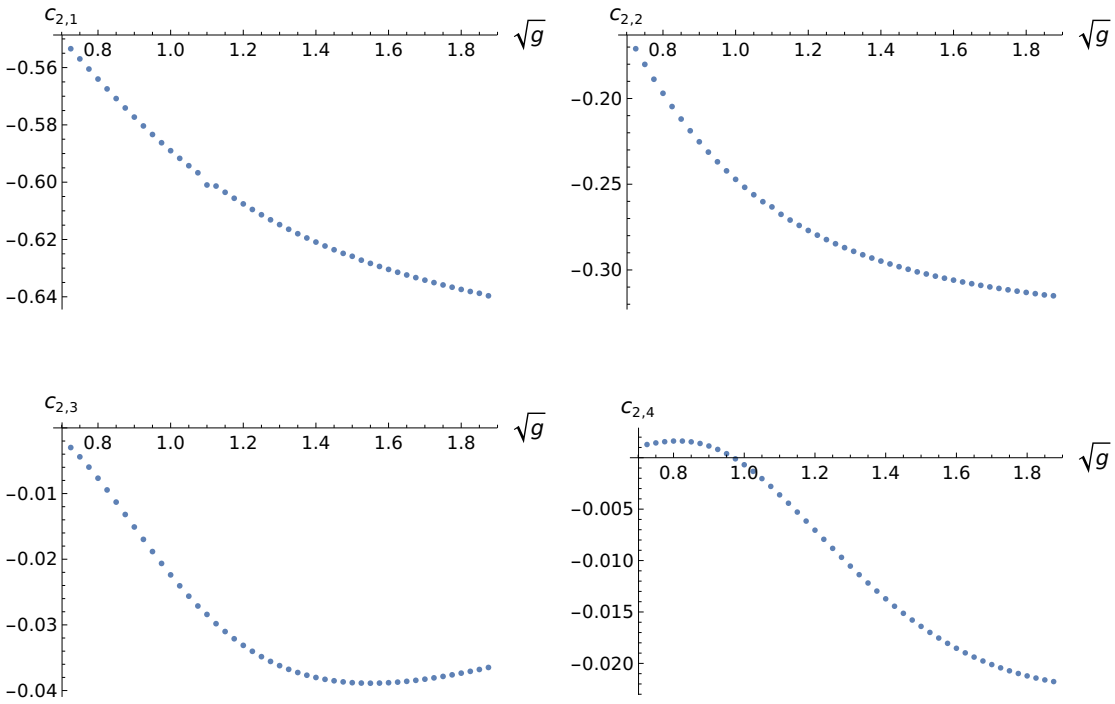

Figure 24: The first four coefficients of $\mathbf{Q}_2(u)$ eq. (131) plotted as a function of $\sqrt{g}$.

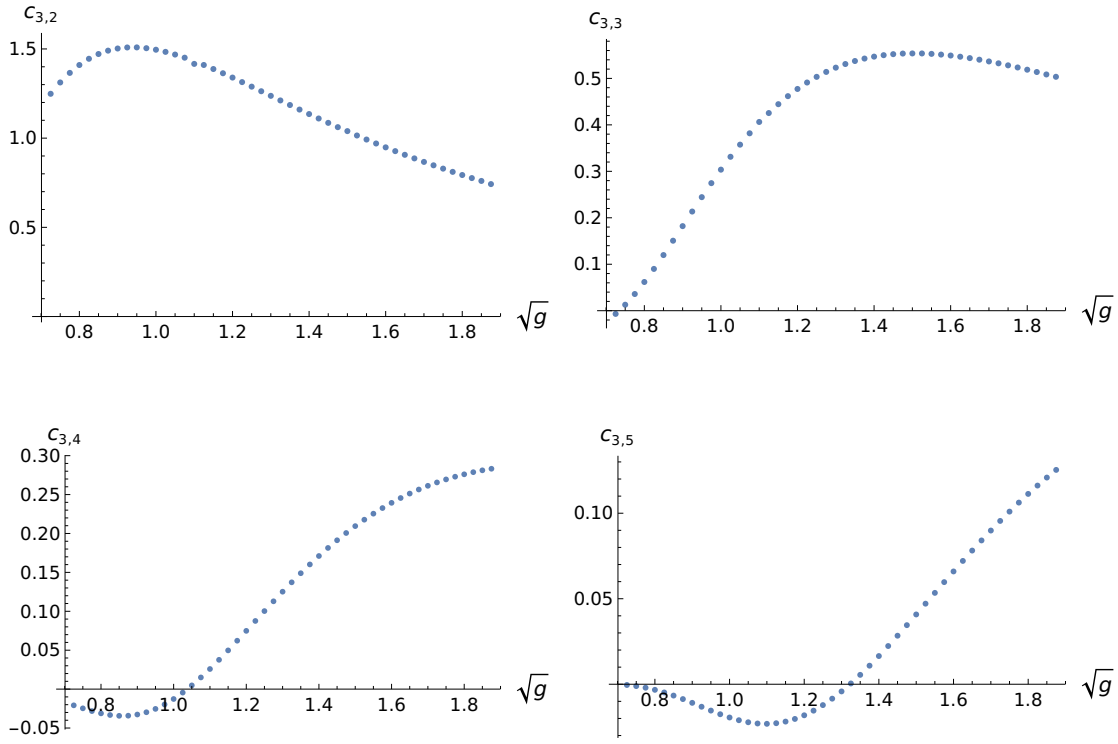

Figure 25: The first four coefficients of $\mathbf{Q}_3(u)$ eq. (131) plotted as a function of $\sqrt{g}$. $c_{3,1}$ is set to zero as explained in section 2.3.4.

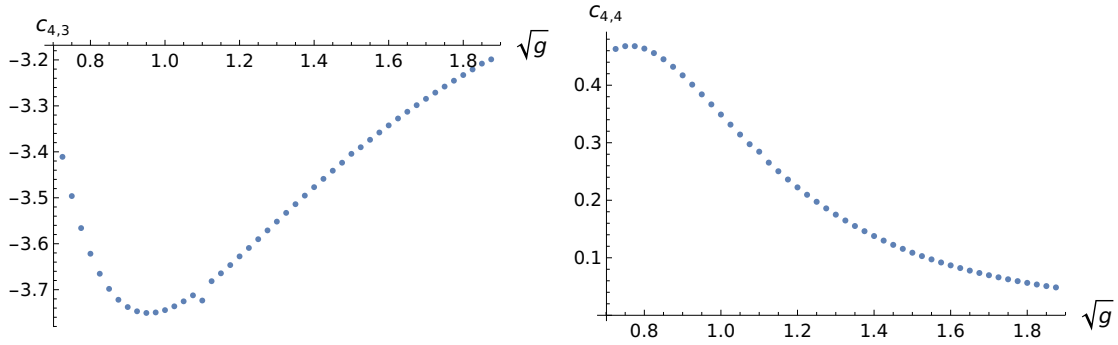

Figure 26: The third and fourth coefficients of $\mathbf{Q}_4(u)$ eq. (131) plotted as a function of $\sqrt{g}$.

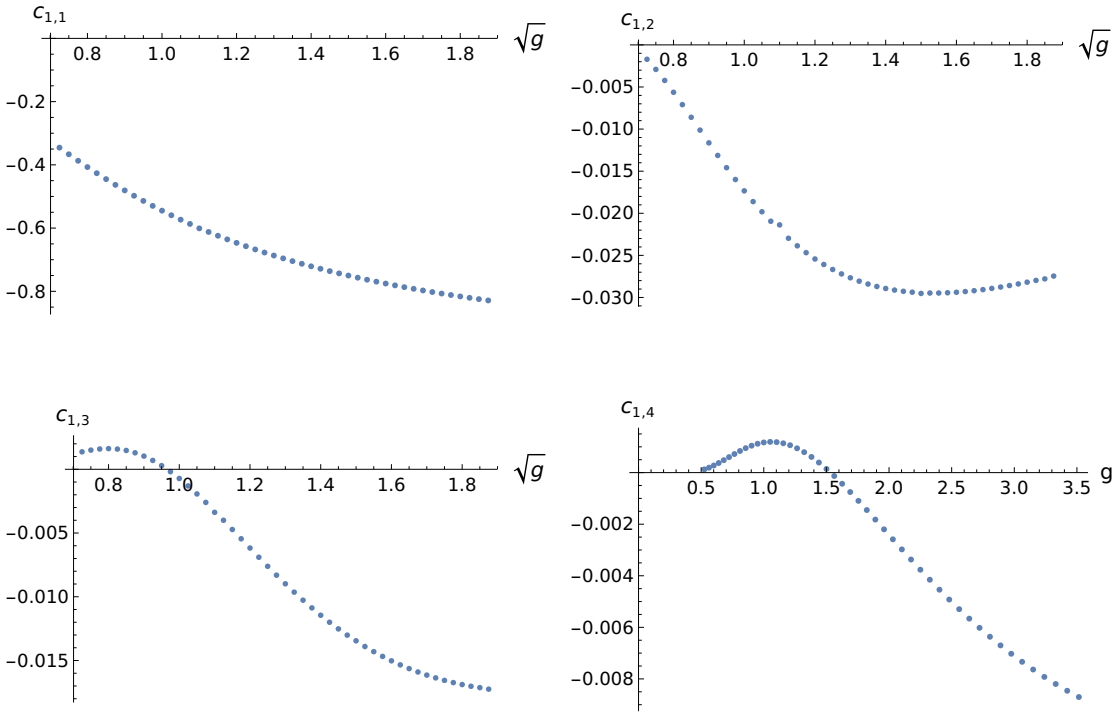

Figure 27: The first four coefficients of $\mathbf{Q}_1(u)$ eq. (131) plotted as a function of g.

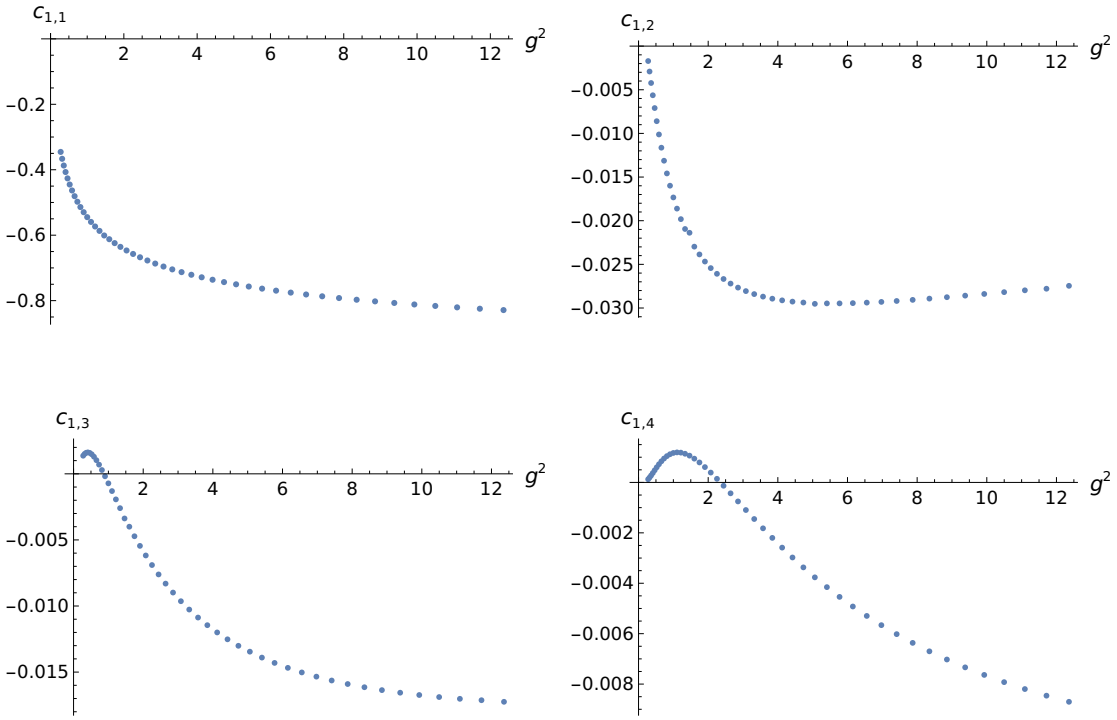

Figure 28: The first four coefficients of $\mathbf{Q}_1(u)$ eq. (131) plotted as a function of g^2.

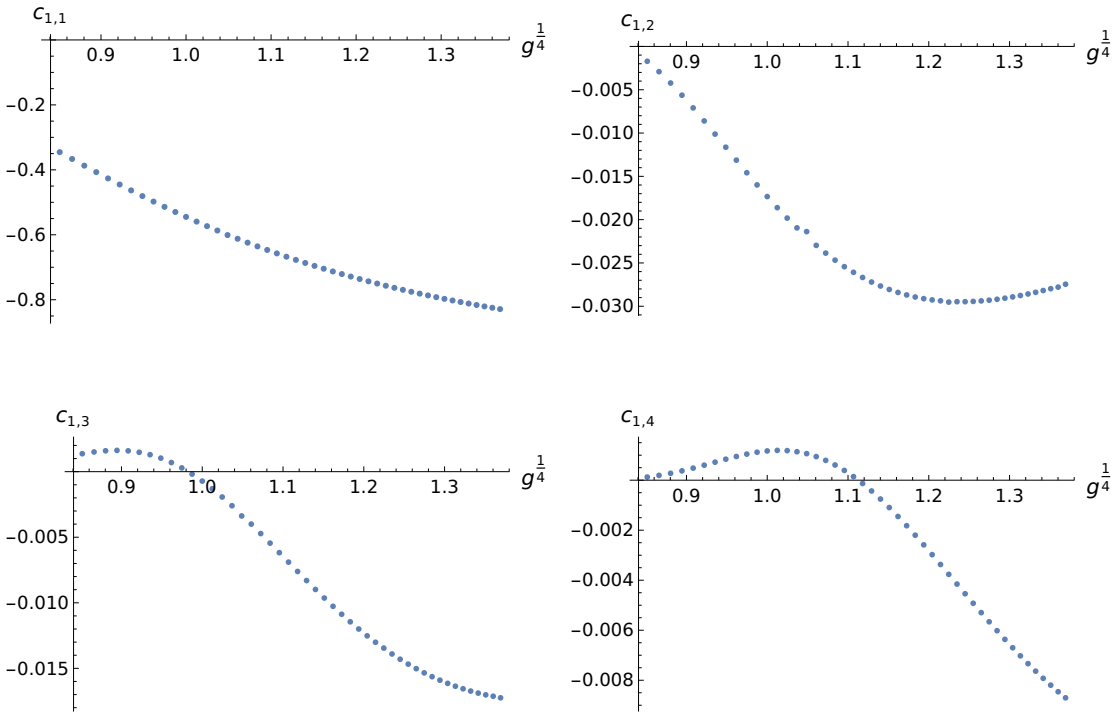

Figure 29: The first four coefficients of $\mathbf{Q}_1(u)$ eq. (131) plotted as a function of $g^{\frac{1}{4}}$.

Table 4: Table of the leading order coefficient b_0 for the coefficients $a_{a,l}$ defined as eqs. (165) and (166). The columns show different orders of correction terms $\frac{1}{\sqrt{g}}$.

	0.	1.	2.	3.	4.	5.	6.
$a_{1,0}$	-2.10119	-2.1961	-2.2468	-2.2954	-2.33523	-2.31317	-2.33572
$a_{2,0}$	-2.11028	-2.22598	-2.25691	-2.29458	-2.33477	-2.312	-2.34658
$a_{1,1}$	-4.02582	-3.25339	-2.96196	-2.85091	-2.86865	-1.81126	-13.2613
$a_{2,1}$	-4.04787	-3.2743	-2.96265	-2.84488	-2.84894	-1.38396	-14.446

Table 5: Table of the leading order coefficient b for the coefficients $a_{a,l}$ defined as eq. (167). The columns show different orders of correction terms $\frac{1}{\sqrt{g}}$.

	0.	1.	2.	3.	4.	5.	6.	7.
$a_{1,0}$	-2.06641	-2.17233	-0.927896	-1.24612	-1.42009	-1.63121	-2.08836	-1.45113
$a_{2,0}$	-2.06684	-2.20554	-0.965216	-1.29011	-1.4439	-1.65266	-2.09438	-1.49147
$a_{1,1}$	-4.2512	-3.46086	-2.80371	-2.78012	-3.71924	-3.33696	-5.30077	-4.81567
$a_{2,1}$	-4.27398	-3.48318	-2.62711	-2.821	-0.475266	-3.41779	-5.44683	-4.95569

Table 6: Table of the exponent coefficient b for the coefficients $a_{3,l}$ and $a_{4,l}$ defined as eq. (169). The columns show different orders of correction terms $\frac{1}{g}$.

	0.	1.	2.	3.	4.	5.	6.	7.
$a_{3,0}$	-1.16578	-1.31155	-1.41252	-1.49057	-1.5617	-1.63254	-1.67588	-1.62008
$a_{4,0}$	-1.22425	-1.34388	-1.43626	-1.51041	-1.57643	-1.6421	-1.68516	-1.6474
$a_{3,1}$	-2.40589	-2.41967	-2.33384	0.0157163	-2.52507	-2.52507	-4.35182	-6.7231
$a_{4,1}$	-2.50817	-2.45005	-0.855504	-3.13898	-2.49326	-4.23644	-6.58695	-5.7474

References

[1] T. Harmark and M. Wilhelm, "The Hagedorn temperature of AdS_5/CFT_4 at finite coupling via the Quantum Spectral Curve," *Phys. Lett. B* **786** (2018) 53–58, arXiv:1803.04416 [hep-th].

[2] S. W. Hawking, "Particle Creation by Black Holes,".

[3] G. 't Hooft, "Dimensional reduction in quantum gravity," *Conf. Proc. C* **930308** (1993) 284–296, arXiv:gr-qc/9310026.

[4] L. Susskind, "The World as a hologram," *J. Math. Phys.* **36** (1995) 6377–6396, arXiv:hep-th/9409089.

[5] J. M. Maldacena, "The Large N limit of superconformal field theories and supergravity," *Adv. Theor. Math. Phys.* **2** (1998) 231–252, arXiv:hep-th/9711200.

[6] E. Witten, "Anti-de Sitter space and holography," *Adv. Theor. Math. Phys.* **2** (1998) 253–291, arXiv:hep-th/9802150.

[7] E. Witten, "Anti-de Sitter space, thermal phase transition, and confinement in gauge theories," *Adv. Theor. Math. Phys.* **2** (1998) 505–532, arXiv:hep-th/9803131.

[8] O. Aharony, O. Bergman, D. L. Jafferis, and J. Maldacena, "N=6 superconformal Chern-Simons-matter theories, M2-branes and their gravity duals," *JHEP* **10** (2008) 091, arXiv:0806.1218 [hep-th].

[9] M. Guica, T. Hartman, W. Song, and A. Strominger, "The Kerr/CFT Correspondence," *Phys. Rev. D* **80** (2009) 124008, arXiv:0809.4266 [hep-th].

[10] H. Liu, K. Rajagopal, and U. A. Wiedemann, "Wilson loops in heavy ion collisions and their calculation in AdS/CFT," *JHEP* **03** (2007) 066, arXiv:hep-ph/0612168.

[11] A. Buchel and J. T. Liu, "Universality of the shear viscosity in supergravity," *Phys. Rev. Lett.* **93** (2004) 090602, arXiv:hep-th/0311175.

[12] H. Liu, K. Rajagopal, and U. A. Wiedemann, "Calculating the jet quenching parameter from AdS/CFT," *Phys. Rev. Lett.* **97** (2006) 182301, arXiv:hep-ph/0605178.

[13] S. A. Hartnoll, P. K. Kovtun, M. Muller, and S. Sachdev, "Theory of the Nernst effect near quantum phase transitions in condensed matter, and in dyonic black holes," *Phys. Rev. B* **76** (2007) 144502, arXiv:0706.3215 [cond-mat.str-el].

[14] S. A. Hartnoll, C. P. Herzog, and G. T. Horowitz, "Building a Holographic Superconductor," *Phys. Rev. Lett.* **101** (2008) 031601, arXiv:0803.3295 [hep-th].

[15] O. Aharony, J. Marsano, S. Minwalla, K. Papadodimas, and M. Van Raamsdonk, "The deconfinement and Hagedorn phase transitions in weakly coupled large N gauge theories," vol. 5, pp. 945–954. 2004.

[16] B. Lucini, M. Teper, and U. Wenger, "The Deconfinement transition in SU(N) gauge theories," *Phys. Lett. B* **545** (2002) 197–206, arXiv:hep-lat/0206029.

[17] B. Lucini, M. Teper, and U. Wenger, "The High temperature phase transition in SU(N) gauge theories," *JHEP* **01** (2004) 061, arXiv:hep-lat/0307017.

[18] B. Sundborg, "The Hagedorn transition, deconfinement and N=4 SYM theory," *Nucl. Phys. B* **573** (2000) 349–363, arXiv:hep-th/9908001.

[19] J. A. Minahan and K. Zarembo, "The Bethe ansatz for N=4 superYang-Mills," *JHEP* **03** (2003) 013, arXiv:hep-th/0212208.

[20] I. Bena, J. Polchinski, and R. Roiban, "Hidden symmetries of the AdS(5) x S**5 superstring," *Phys. Rev. D* **69** (2004) 046002, arXiv:hep-th/0305116.

[21] N. Gromov, V. Kazakov, S. Leurent, and D. Volin, "Solving the AdS/CFT Y-system," *JHEP* **07** (2012) 023, arXiv:1110.0562 [hep-th].

[22] N. Beisert, "The Dilatation operator of N=4 super Yang-Mills theory and integrability," *Phys. Rept.* **405** (2004) 1–202, arXiv:hep-th/0407277.

[23] M. Ammon and J. Erdmenger, *Gauge/Gravity Duality: Foundations and Applications*. Cambridge University Press, 2015.

[24] O. Aharony, S. S. Gubser, J. M. Maldacena, H. Ooguri, and Y. Oz, "Large N field theories, string theory and gravity," *Phys. Rept.* **323** (2000) 183–386, arXiv:hep-th/9905111.

[25] M. F. Sohnius and P. C. West, "Conformal Invariance in N=4 Supersymmetric Yang-Mills Theory," *Phys. Lett. B* **100** (1981) 245.

[26] L. Brink, O. Lindgren, and B. E. W. Nilsson, "The Ultraviolet Finiteness of the N=4 Yang-Mills Theory," *Phys. Lett. B* **123** (1983) 323–328.

[27] S. Ferrara and B. Zumino, "Supergauge Invariant Yang-Mills Theories," *Nucl. Phys. B* **79** (1974) 413.

[28] D. R. T. Jones, "Charge Renormalization in a Supersymmetric Yang-Mills Theory," *Phys. Lett. B* **72** (1977) 199–199.

[29] E. C. Poggio and H. N. Pendleton, "Vanishing of Charge Renormalization and Anomalies in a Supersymmetric Gauge Theory," *Phys. Lett. B* **72** (1977) 200.

[30] L. V. Avdeev, O. V. Tarasov, and A. A. Vladimirov, "VANISHING OF THE THREE LOOP CHARGE RENORMALIZATION FUNCTION IN A SUPERSYMMETRIC GAUGE THEORY," *Phys. Lett. B* **96** (1980) 94–96.

[31] M. B. Green, J. H. Schwarz, and L. Brink, "N=4 Yang-Mills and N=8 Supergravity as Limits of String Theories," *Nucl. Phys. B* **198** (1982) 474–492.

[32] S. Mandelstam, "Light Cone Superspace and the Ultraviolet Finiteness of the N=4 Model," *Nucl. Phys. B* **213** (1983) 149–168.

[33] J. A. Minahan, "Review of AdS/CFT Integrability, Chapter I.1: Spin Chains in N=4 Super Yang-Mills," *Lett. Math. Phys.* **99** (2012) 33–58, arXiv:1012.3983 [hep-th].

[34] R. Haag, J. T. Lopuszanski, and M. Sohnius, "All Possible Generators of Supersymmetries of the s Matrix," *Nucl. Phys. B* **88** (1975) 257.

[35] G. 't Hooft, "A Planar Diagram Theory for Strong Interactions," *Nucl. Phys. B* **72** (1974) 461.

[36] N. Beisert, C. Kristjansen, and M. Staudacher, "The Dilatation operator of conformal N=4 superYang-Mills theory," *Nucl. Phys. B* **664** (2003) 131–184, arXiv:hep-th/0303060.

[37] D. E. Berenstein, J. M. Maldacena, and H. S. Nastase, "Strings in flat space and pp waves from N=4 Super Yang Mills," *AIP Conf. Proc.* **646** no. 1, (2002) 3–14.

[38] D. J. Gross, A. Mikhailov, and R. Roiban, "Operators with large R charge in N=4 Yang-Mills theory," *Annals Phys.* **301** (2002) 31–52, arXiv:hep-th/0205066.

[39] S. W. Hawking and D. N. Page, "Thermodynamics of Black Holes in anti-De Sitter Space," *Commun. Math. Phys.* **87** (1983) 577.

[40] S. S. Gubser, I. R. Klebanov, and A. M. Polyakov, "Gauge theory correlators from noncritical string theory," *Phys. Lett. B* **428** (1998) 105–114, arXiv:hep-th/9802109.

[41] J. M. Maldacena, "Wilson loops in large N field theories," *Phys. Rev. Lett.* **80** (1998) 4859–4862, arXiv:hep-th/9803002.

[42] S. Ryu and T. Takayanagi, "Holographic derivation of entanglement entropy from AdS/CFT," *Phys. Rev. Lett.* **96** (2006) 181602, arXiv:hep-th/0603001.

[43] C. B. Thorn, "INFINITE N(c) QCD AT FINITE TEMPERATURE: IS THERE AN ULTIMATE TEMPERATURE?," *Phys. Lett. B* **99** (1981) 458–462.

[44] C. P. Burgess, N. R. Constable, and R. C. Myers, "The Free energy of N=4 superYang-Mills and the AdS / CFT correspondence," *JHEP* **08** (1999) 017, arXiv:hep-th/9907188.

[45] S. S. Gubser, I. R. Klebanov, and A. W. Peet, "Entropy and temperature of black 3-branes," *Phys. Rev. D* **54** (1996) 3915–3919, arXiv:hep-th/9602135.

[46] R. Hagedorn, "Statistical thermodynamics of strong interactions at high-energies," *Nuovo Cim. Suppl.* **3** (1965) 147–186.

[47] M. Panero, "Recent results in large-N lattice gauge theories," *PoS* **LATTICE2012** (2012) 010, arXiv:1210.5510 [hep-lat].

[48] G. Curci and G. Veneziano, "Supersymmetry and the Lattice: A Reconciliation?," *Nucl. Phys. B* **292** (1987) 555–572.

[49] S. Catterall, D. B. Kaplan, and M. Unsal, "Exact lattice supersymmetry," *Phys. Rept.* **484** (2009) 71–130, arXiv:0903.4881 [hep-lat].

[50] S. A. Abel, J. L. F. Barbon, I. I. Kogan, and E. Rabinovici, "String thermodynamics in D-brane backgrounds," *JHEP* **04** (1999) 015, arXiv:hep-th/9902058.

[51] S. A. Abel, J. L. F. Barbon, I. I. Kogan, and E. Rabinovici, "Some thermodynamical aspects of string theory," arXiv:hep-th/9911004.

[52] C. R. Graham and J. M. Lee, "Einstein metrics with prescribed conformal infinity on the ball," *Adv. Math.* **87** no. 2, (1991) 186–225.

[53] D. Berenstein, "Submatrix deconfinement and small black holes in AdS," *JHEP* **09** (2018) 054, arXiv:1806.05729 [hep-th].

[54] G. Polya, *Combinatorial enumeration of groups, graphs, and chemical compounds.* Springer-Verlag, New York, 1987.

[55] T. Harmark and M. Wilhelm, "Hagedorn Temperature of AdS_5/CFT_4 via Integrability," *Phys. Rev. Lett.* **120** no. 7, (2018) 071605, arXiv:1706.03074 [hep-th].

[56] R. R. Metsaev and A. A. Tseytlin, "Type IIB superstring action in AdS(5) x S**5 background," *Nucl. Phys. B* **533** (1998) 109–126, arXiv:hep-th/9805028.

[57] L. F. Alday, G. Arutyunov, and A. A. Tseytlin, "On integrability of classical superstrings in AdS(5) x S**5," *JHEP* **07** (2005) 002, arXiv:hep-th/0502240.

[58] K. Zarembo, "Integrability in Sigma-Models," arXiv:1712.07725 [hep-th].

[59] G. Arutyunov and S. Frolov, "Foundations of the $AdS_5 \times S^5$ Superstring. Part I," *J. Phys. A* **42** (2009) 254003, arXiv:0901.4937 [hep-th].

[60] N. Gromov and P. Vieira, "The AdS(5) x S**5 superstring quantum spectrum from the algebraic curve," *Nucl. Phys. B* **789** (2008) 175–208, arXiv:hep-th/0703191.

[61] N. Beisert, V. A. Kazakov, K. Sakai, and K. Zarembo, "The Algebraic curve of classical superstrings on AdS(5) x S**5," *Commun. Math. Phys.* **263** (2006) 659–710, arXiv:hep-th/0502226.

[62] N. Gromov, V. Kazakov, A. Kozak, and P. Vieira, "Exact Spectrum of Anomalous Dimensions of Planar N = 4 Supersymmetric Yang-Mills Theory: TBA and excited states," *Lett. Math. Phys.* **91** (2010) 265–287, arXiv:0902.4458 [hep-th].

[63] D. Bombardelli, D. Fioravanti, and R. Tateo, "Thermodynamic Bethe Ansatz for planar AdS/CFT: A Proposal," *J. Phys. A* **42** (2009) 375401, arXiv:0902.3930 [hep-th].

[64] G. Arutyunov and S. Frolov, "Thermodynamic Bethe Ansatz for the AdS(5) x S(5) Mirror Model," *JHEP* **05** (2009) 068, arXiv:0903.0141 [hep-th].

[65] N. Gromov, V. Kazakov, and P. Vieira, "Exact Spectrum of Anomalous Dimensions of Planar N=4 Supersymmetric Yang-Mills Theory," *Phys. Rev. Lett.* **103** (2009) 131601, arXiv:0901.3753 [hep-th].

[66] N. Gromov, V. Kazakov, S. Leurent, and Z. Tsuboi, "Wronskian solution for ads/cft y-system," *Journal of High Energy Physics* **2011** no. 1, (Jan, 2011) . http://dx.doi.org/10.1007/JHEP01(2011)155.

[67] N. Gromov, "Introduction to the Spectrum of $N = 4$ SYM and the Quantum Spectral Curve," arXiv:1708.03648 [hep-th].

[68] H. Bethe, "On the theory of metals. 1. Eigenvalues and eigenfunctions for the linear atomic chain," vol. 71, pp. 205–226. 1931.

[69] N. Beisert, "The complete one loop dilatation operator of N=4 superYang-Mills theory," *Nucl. Phys. B* **676** (2004) 3–42, arXiv:hep-th/0307015.

[70] N. Beisert, "The su(2—3) dynamic spin chain," *Nucl. Phys. B* **682** (2004) 487–520, arXiv:hep-th/0310252.

[71] R. J. Baxter, "Completeness of the Bethe ansatz for the six and eight vertex models," *J. Statist. Phys.* **108** (2002) 1–48, arXiv:cond-mat/0111188.

[72] F. Levkovich-Maslyuk, "A review of the AdS/CFT Quantum Spectral Curve," *J. Phys. A* **53** no. 28, (2020) 283004, arXiv:1911.13065 [hep-th].

[73] N. Gromov, V. Kazakov, S. Leurent, and D. Volin, "Quantum spectral curve for arbitrary state/operator in AdS_5/CFT_4," *JHEP* **09** (2015) 187, arXiv:1405.4857 [hep-th].

[74] V. Kazakov, A. Sorin, and A. Zabrodin, "Supersymmetric bethe ansatz and baxter equations from discrete hirota dynamics," *Nuclear Physics B* **790** no. 3, (Feb, 2008) 345–413. http://dx.doi.org/10.1016/j.nuclphysb.2007.06.025.

[75] V. Kazakov, S. Leurent, and D. Volin, "T-system on T-hook: Grassmannian Solution and Twisted Quantum Spectral Curve," *JHEP* **12** (2016) 044, arXiv:1510.02100 [hep-th].

[76] N. Gromov, F. Levkovich-Maslyuk, and G. Sizov, "Quantum Spectral Curve and the Numerical Solution of the Spectral Problem in AdS5/CFT4," *JHEP* **06** (2016) 036, arXiv:1504.06640 [hep-th].

[77] B. Sundborg, "Thermodynamics of Superstrings at High-energy Densities," *Nucl. Phys. B* **254** (1985) 583–592.